Studies on Cantilever Energy Harvester under Harmonic and Random Excitations

Kattamanchi Manoj
Roll No. 714022

Mechanical Engineering Department
NATIONAL INSTITUTE OF TECHNOLOGY WARANGAL
2021

Studies on Cantilever Energy Harvester under Harmonic and Random Excitations

Submitted in partial fulfilment of the requirements for the degree of

Doctor of Philosophy

by

Kattamanchi Manoj
Roll No. 714022

Supervisors
Dr. Srikanth Korla
Dr. V. Narayanamurthy

Mechanical Engineering Department
NATIONAL INSTITUTE OF TECHNOLOGY WARANGAL
2021

Thesis approval for PhD

This Dissertation work entitled **"Studies on Cantilever Energy Harvester under Harmonic and Random Excitations"** by **Kattamanchi Manoj** is approved for the
degree of Doctor of Philosophy

Examiners

_____

_____

_____

Supervisors

Dr. Srikanth Korla

Dr. V. Narayanamurthy

Chairman

Prof. Adepu Kumar

Date: _____ Place: _____

Abstract

The technique of harvesting energy from vibration of a structure known as *vibration energy harvesting* is gaining more popularity in recent years. This is achieved by mounting a piezoelectric transducer at an appropriate location on the structure. The amount of energy harvested depends on the type and magnitude of excitation on the base structure. The vibration levels that excite the harvester vary depending upon the application or the base structure on which the harvester is mounted. The vibration can be with single harmonic source, multiple harmonic source, a repeating step / ramp excitation or a random vibration with continuously varying frequencies in a given frequency range. Although several researches exist on energy harvesting from harmonic excitations and few from random excitations of base structure, the energy harvested under random excitation as compared to equivalent harmonic excitations is not yet well understood. This thesis is devoted to understand this difference and is investigated through a cantilever energy harvester (CEH).

Initially, the numerical simulation is carried out on Cantilever energy harvester under increasing magnitude of harmonic excitation for different loads. Experiments are conducted for same conditions whose results are in good agreement with simulations. Subsequently, the performance of this energy harvester is experimentally studied under random excitations. The results explain that the harvested power (a) reaches maximum value when the harvester is in resonance with base excitation, (b) Irrespective of the type of excitation, increases with increase in magnitude of base excitation and (c) increases by 2-14 times in random excitations as compared to equivalent harmonic excitations for the same energy input.

Subsequently, in order to have more understanding on the behavior of CEH during its practical application, the CEH is mounted inside an airframe section and subjected to separate harmonic and random excitations. The results demonstrated that the (a) CEH produces more power at lower base excitation frequency bandwidths when acceleration levels are higher and load resistances are minimal, (b) energy harvested in the random excitation with minimum frequency bandwidth is comparatively higher than that in equivalent harmonic excitation unlike the case in which energy harvested under harmonic excitation is more than that under random excitation with higher frequency bandwidth.

Keywords: Vibration, piezoelectric transducer, harmonic excitation, random excitation

Declaration

This is to certify that the work presented in the thesis entitled **Studies on Cantilever Energy Harvester under Harmonic and Random Excitations** is a bonafide work done by me under the supervision of Dr. Srikanth Korla and Dr. V. Narayanamurthy and was not submitted elsewhere for the award of any degree.

I declare that this written submission represents my ideas in my own words and where others' ideas or words have been included, I have adequately cited and referenced the original sources. I also declare that I have adhered to all principles of academic honesty and integrity and have not misrepresented or fabricated or falsified any idea / data / fact / source in my submission. I understand that any violation of the above will be a cause for disciplinary action by the Institute and can also evoke penal action from the sources which have thus not been properly cited or from whom proper permission has not been taken when needed.

_____

(Signature)

Kattamanchi Manoj

(Name of the student)

714022

(Roll No.)

Date: _____

Acknowledgements

I would like to offer my sincerest gratitude to the Director, RCI and Shri Gopinath, OS, RCI for giving me the opportunity to conduct research in the form of PhD on Vibration energy harvesting.

I am very thankful to Dr. Srikanth Korla, my thesis supervisor (Internal) who paid a great deal of patience in not only guiding during the research but also teaching the courses Product design and piezoelectric energy harvesting and gave innovative inputs that were very useful during the research.

I want to thank Dr. Vijayabaskar Narayanamurthy, my thesis supervisor (External) who motivated, encouraged and gave me detailed guidance while conceptualizing the problem and carrying out experiments.

I take this opportunity to thank Smt. Ammani, Technical Officer at RCI for supporting me in preparing the specimens for energy harvesting.

I want to thank Shri Bhaskar, Shri Sai Kiran, Shri Vishweshwar and Shri Manikiran for supporting me with required infrastructure for carrying out the experiments.

I want to say thanks to Shri EV Subba Rao and Shri Raghavendra, Scientists from RCI for providing me the required Data Acquisition System for carrying out the experiments and Shri Jayakrishna for supporting with required information during experiments.

I thank my family, who always concern with my personal growth, and encourage me to pursue my career and dreams. Especially I want to say thank you to my parents, who has showed generous love to me. They with their wisdom can always guide me and take away my pressure.

Kattamanchi Manoj

Table of Contents

List of Figures

List of Tables

List of Symbols

b	:	Width of beam (mm)
CEH	:	Cantilever Energy Harvester
C_p^{eq}	:	Internal capacitance (C)
D_3	:	Electric displacement component (C/m^2)
E	:	Young's modulus of elasticity (MPa)
E_3	:	Electric field in the direction of thickness (V/m)
e_{31}	:	Piezoelectric stress constant(C/m^2)
EH	:	Energy Harvester
EHS	:	Energy Harvesting Structure
FEA	:	Finite Element Analysis
F_r	:	Forcing function (N)
f_r	:	rth natural frequency (Hz)
g(t)	:	Transverse base displacement of beam (mm)
h(t)	:	Base rotation of beam (Rad)
h_p	:	Thickness of piezoelectric layer (mm)
h_s	:	Thickness of substructure (mm)
I	:	Moment of Inertia (mm^4)
i	:	Current (A)
M_t	:	Proof mass (kg)
PVDF	:	Polyvinylidene fluoride
PZT	:	Lead Zirconate Titanate
R	:	Load resistance (Ohm)
S_0	:	Power spectral density (g^2/Hz)
V(t)	:	Voltage (V)
w	:	Transverse dispalcement (mm)
w_b (x,t)	:	Base displacement (mm)
w_{rel} (x,t) :	:	Transverse tip displacement (mm)
$\delta_1(x)$	:	Displacement influence functions for the transverse base displacement
$\delta_2(x)$	:	Displacement influence functions for the small base rotation of the beam
ε_{33}^s	:	Permittivity component at constant strain (f/m)
ζ_r	:	Damping factor
η_r	:	rth Modal parameter
θ_r	:	Modal electro-mechanical coupling parameter
μ	:	Voltage output to rotational base acceleration
σ_b	:	Bending stress (MPa)
$\Phi_r(x)$	:	rth Eigen function

Publications from Thesis

Peer Reviewed Journals

1. K. Manoj, V. Narayanamurthy and S. Korla, Analysis and characterisation of a cantilever energy harvester, *Journal of Structural Engineering*, Vol. 45, No. 1, pp 10-20, 2018.
2. K. Manoj, V. Narayanamurthy and S. Korla, Performance of a cantilever energy harvester under harmonic and random excitations, *Defence Science Journal*, Vol. 71, No. 2, pp. 231-240, 2021.
3. K. Manoj, V. Narayanamurthy and S. Korla, Simulations and experiments on an energy harvester under harmonic excitations, *NMIMS Journal of Engineering and Technology Review*, Vol. 3, pp 27-41, 2021.
4. K. Manoj, V. Narayanamurthy and S. Korla, Excitation bandwidth dependence of cantilever energy harvester, *Recent Advances in Applied Mechanics, Springer Nature,* pp 1- 18, 2022.

Peer Reviewed International and National Conferences

1. K. Manoj, V. Narayanamurthy and S. Korla, Effect of base acceleration on a cantilever energy harvester, *Proceedings of 3rd Indian National Conference on Applied Mechanics (INCAM-2017),* MNNIT, Allahabad, July 5-7, 2017.
2. K. Manoj, V. Narayanamurthy and S. Korla, Experimental studies on vibration energy harvester under harmonic and random excitations, *Proceedings of 4th Indian National Conference on Applied Mechanics (INCAM-2019),* IISc Bangalore, July 3-5, 2019.

1

Introduction

1.1. Background

The aerospace vehicle will have specific fuel consumption depending on its payload mass to reach the specified destination. If the mass is comparatively more, then either its fuel consumption is more or its range of travel will be less. These vehicles carry some systems that consume the power in terms of milli or micro Watt. The systems are connected by electrical cables to the batteries kept away for these specific requirements. There are certain limitations if we go with conventional way of supplying power to the systems. That is (a) charging and discharging of batteries regularly, (b) disposal of chemical waste after the shelf life of battery, (c) timely replacement of primary batteries, (d) slow rate of installation, and (e) separate cables for power and communication to and from the systems. These systems are required to be operated only when the flight vehicle is in motion. There was a thought process to (a) check whether the mass of the complete vehicle can be brought down to increase the range by resizing the existing battery and removing the cables, and (b) to reduce the maintenance time and cost of the systems based on battery and electrical cables for power supply and communication.

This can be achieved by using the wireless systems. The installation of this system can be simple and fast. The configuration can be flexible. All these can be done by tapping the energy available in the ambience. The sources for the ambient energies may be vibration, temperature, light and fluid flow.

1.2. Motivation

As mentioned in the background, the approach is to reduce the mass, maintenance time and cost of the aerospace vehicle by replacing part of chemical source of power supply (i.e. battery) by tapping energy from ambient temperature and vibration and removing the electrical cables. The focus of the present study is on tapping the energy from ambient vibration. The aerospace vehicle is subjected to undue structural vibrations mainly due to aerodynamic disturbances and its propulsion systems. The aerodynamic disturbances are uncertain depending upon the density of air and atmospheric pressure at a particular altitude and hence random in nature. The propulsion system may be (a) engine which has a compressor and nozzle that causes vibration which is harmonic in nature, and (b) solid and liquid propulsion system that carry fuel and oxidizer and once ignited will generate vibrations which are random in nature along with thrust.

The literature review revealed that there are very limited studies on behavior of energy harvesting structure (EHS) under the influence of random vibration. Even the characterization of EHS for maximum power output under random vibration is not yet well understood. Further, no literature is available on performance of EHS under the influence of both harmonic and random vibrations. These gaps in research motivated not only to quantify the energy harvested from random vibrations that are caused due to aerodynamic disturbances and propulsion but also tried to consider these undesired vibrations as boon instead of penalty.

1.3. Objectives

In order to understand the behavior of EHS under harmonic and random excitations and to evaluate the relative performance of EHS under both excitations, studies are carried out using a cantilever energy harvester as shown in Figure 1.1 [30].

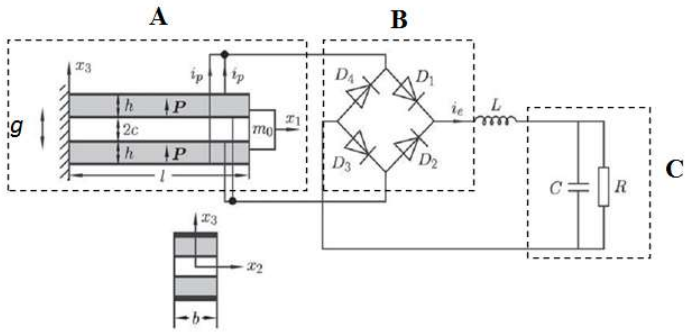

(A: Harvesting structure; B: Rectifying circuit; C: Load)

Figure 1.1. Line diagram of typical energy harvester

Where, h, 2c are thickness of piezoelectric material and sub structure respectively, i_p and i_e is current in circuits, m_0 is tip or proof mass, D_1, D_2, D_3 and D_4 are diodes, L, C and R are inductance, capacitance and resistance respectively.

The objectives of the present research are as summarized below.

i. Numerical simulation of an energy harvester (EH) under harmonic excitation.
ii. Characterisation of EH under harmonic excitation.
iii. Experimental validation of EH under harmonic excitation and comparison with numerical solutions.
iv. Performance evaluation of EH under both harmonic and random excitations - experimental and numerical.
v. Implementation of the EH in an airframe subjected to individual harmonic and random excitations and assessment of the performance.

1.4. Organization of Thesis

The thesis starts with the Chapter-1 that elaborates the statement of problem on which the investigation has been done followed by literature review in Chapter-2 where the details of previous works carried out by different scholars in this field of research is elaborated. The Chapter-3 deals with the formulations for the cantilever beam-based energy harvesting system with assumptions, governing differential equations, boundary conditions and forcing functions depending on the kind of excitation. The equation is solved theoretically and solutions are presented for further reference.

The Chapter-4 discusses about the Numerical simulation work carried out on bimorph cantilever beam-based energy harvesting structure for its characterization and verified with literature for obtaining good understanding.

The Chapter-5 elaborates the work carried out for design of cantilever beam-based energy harvesting structure based on the hardware available and experiments performed on it.

The chapter-6 extends the experimental procedure on the same harvesting structure under random excitation and evaluates the performance of harvesting structure under harmonic and random excitation.

The Chapter-7 discusses the performance of energy harvester when mounted in the flight airframe section by quantifying the power generated when subjected to random vibrations. The complete work is summarized and concluded in Chapter 8.

2

Literature Review

2.1. Introduction

A study on cantilever energy harvester under harmonic and random excitation is required to be carried out in order to understand the characteristics of any typical harvesting structure. There is more emphasis on harmonic and random excitations because in physical life these are the only excitations to which all the structure are subjected to. This study will path the way to application in the field of wireless sensor networks where the challenges like a) charging and discharging of batteries regularly, b) disposal of chemical waste after the shelf life of battery, c) timely replacement of primary batteries, d) slow rate of installation, and e) separate cables for communication to and from the systems, can be addressed. In the process of building knowledge, the literature review is a fundamental requirement of all research projects.

2.2. Techniques of energy harvesting

Different energy harvesting methods from ambience is referred in [1]. The details are as shown in Table 2.1.

Table 2. 1. Energy harvesting from ambient surroundings

S. No.	Energy source	Example	Energy level	Conversion mechanism
1	Ambient radiation	RF signal	< 1 $\mu W/cm^2$	Electromagnetic
2	Ambient light	Sunlight, Illumination	100 mW/cm^2 (bright sunlight) 100 $\mu W/cm^2$ (office illumination)	Photovoltaic
3	Vibration	Machine vibration, human motion	4-800 $\mu W/cm^3$	Piezoelectric Electromagnetic Electrostatic
4	Fluid flow	Wind, Ventilation, Piping, Current wave	Air: 200-800 $\mu W/cm^3$	Turbine (Electromagnetic). Piezoelectric
			Water: 500 $\mu W/cm^3$	
5	Thermal	Temperature differential	60 $\mu W/cm^2$ at 5^0 C difference	Thermoelectric Thermionic Thermo-tunneling
6	Pressure variation	Daily atmospheric pressure range	< 10 $\mu W/cm^3$	Unclear

2.3. Classifications of vibration energy harvesters

There are three kinds of transducers [1] that are used for vibration energy harvesting 1) Electromagnetic, 2) Electrostatic and 3) Piezoelectric. These electromagnetic and electrostatic transducer based energy harvesters are applicable for harvesting energy in the cases of vibration that has low frequency range and high amplitude. Whereas the Piezoelectric transducer based energy harvesters are applicable for the cases of vibration that has high frequency ranges and low amplitude.

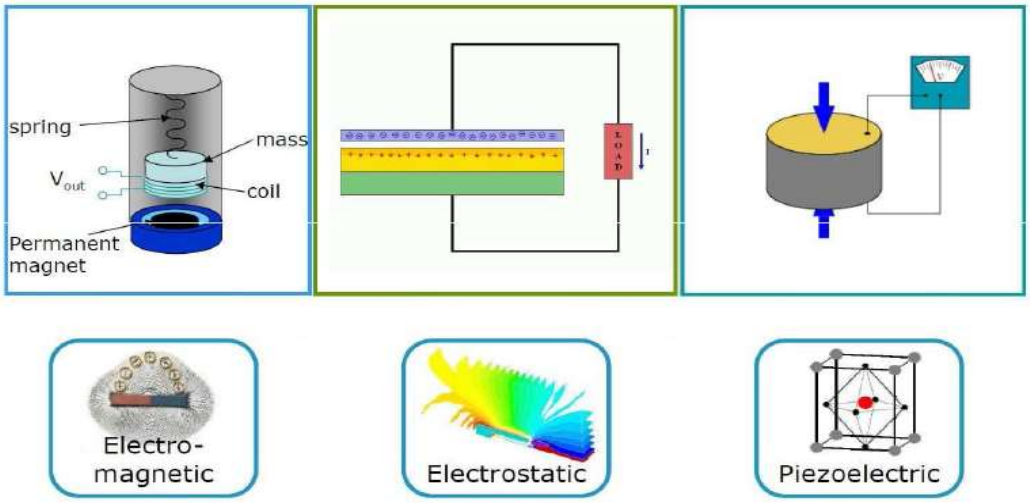

Figure 2.1. Classification of vibration energy harvesting

The advantages of piezoelectric vibration energy harvester over other vibration energy harvesters are:

1. Separate voltage source is not required for operation,
2. Mechanical stops not required, and
3. Has the highest power density

The disadvantages are

1. The fabrication processes are not compatible with standard processes due to their size and
2. Poor coupling of piezo thin films.

2.4. Vibration energy harvesting under different excitations

In general, ambient vibration provides excitation to the energy harvesting system and once the excitation frequency is close to the natural system frequency, a maximum output power is captured. So, the type, amplitude and frequency or frequency bandwidth of excitation are the main inputs to vibration energy harvester. In addition, operating conditions also play a vital role in performance of energy harvester [2]. Based on excitation, the input to energy harvester is classified into harmonic and random excitation. *Harmonic excitation* is a sinusoidal external force of a certain frequency applied to a system. *Random excitation* is a non-deterministic motion whose future behavior cannot be precisely predicted. The randomness is a characteristic of the excitation or input, not the mode shapes or natural frequencies. For harmonic excitation, amplitude and excitation frequency is applicable whereas random excitation is characterized by amplitude and frequency bandwidth.

Ambient vibration is converted to electrical power using MEMS-based energy harvesting device that uses piezo-electric effect. The harvesting device here uses structure made up of composite cantilever with proof mass made up of nickel so as to bring the resonant conditions for low-frequency environmental vibration [3]. One of the application of piezoelectric effect where the backpack generates electrical energy from the differential forces between the wearer and the pack. This is executed by replacing the strap buckle with a mechanically amplified piezoelectric stack actuator [4]. Piezoelectric energy harvester that converts flow induced vibration into electrical energy is also explored [5]. This happens by piezoelectric conversion with oscillation of a piezoelectric film. Most of the piezoelectric energy harvesters that convert harmonic vibration into electrical energy are based on linear mechanical resonators that are efficient when excited at resonance. The performance of such energy harvesters under wideband vibrations are suboptimal.

The study proposes a nonlinear converter consisting of piezoelectric bimorph on a ferromagnetic cantilever that makes use of a magnet for bi-stability and non-linearity to improve conversion effectiveness [6]. The configuration and fabrication of a harvesting device that converts low frequency vibrations with piezoelectric effect is investigated [7]. In this study, PZT (piezoelectric transducer) thin film patterns are arranged in parallel but isolated electrically on a cantilever beam. The performance of harvesting device when PZT patterns are connected electrically in parallel and in series is investigated and found that same level of power is generated in corresponding matched load resistance. The only difference is, in parallel connection, lower matched load resistance is required to generate power compared to that in series connection. The properties of energy harvesting device that is used to harvest energy from the vehicles in traffic, pedestrians and train is studied in [8]. In this study piezoelectric bender transducer is used in place of stack transducer. The vibration energy harvesting using single and comb shaped piezoelectric beam structures is explored in [9]. Experiments were carried out on them in the frequency range of 0 to 3500 kHz. The performance of comb shaped beam structure is comparatively better due to more number of natural frequencies in the range of frequencies. The performance of PZT diaphragm energy harvester is studied in [10]. The harvester is clamped at the periphery that introduces the pre-stress controlling its natural frequency. Zhou *et al.* [11] studied the electrical model that consists of piezoelectric constitutive equations. In this study, the energy harvesting by piezoelectric cantilever in shear mode is studied by using d_{15} mode of constitutive equation and single degree of freedom system. Energy

harvesting due to strain induced in piezoelectric cantilever due to propagation of radio frequency signal is explored in [12]. The piezoelectric cantilever is coupled to radio frequency line through a specified gap. When the voltage signal propagates in the line, it sets an alternating current in the piezoelectric electrodes on cantilever beam. The current induces mechanical strain in the piezoelectric cantilever. The procedure for optimizing topology for designing layouts for piezoelectric energy harvesters based on static and dynamic loads and the coupling effects between electric parameters and structure is established [13]. The procedure consists of determining responses to loads and analyzing the complex sensitivity for various objectives related to efficiency of energy. Wang *et al.* [14] developed an analytical model in which a piezoelectric cantilever is proposed with plug type connection between support layer and proof mass. This configuration of piezoelectric energy harvester is to ensure that there should not be any brittle fracture in it for large amplitudes of vibration. This is achieved by maintaining collinearity between the center of gravity of proof mass and the center of gravity of the beam.

Ashtari *et al.* [15] investigated energy harvester for increasing power generation. The configuration includes an array of three piezoelectric bimorph cantilevers with magnetic tuning. The advantage of present configuration is its insensitivity to manufacturing tolerances as the optimum operation frequency can be tuned after fabrication. Fakhzan *et al.* [16] presents estimate of voltage generated across the load attached to piezoelectric energy harvester when exposed to base excitation. In this study, the energy harvester employs the Euler-Bernoulli's beam and analyzed with and without tip mass. An 'X' shaped piezoelectric energy harvester [17] to generate electric power at low frequencies is explored. This configuration consists of four elastic legs from a single centre that is attached to a source of vibration. These four legs are symmetric in all the three planes, have same natural frequency and hence same modes of vibration. The vibration from source is transferred from center of the energy harvester and is equally transmitted to each elastic leg. The piezoelectric energy harvesting [18] in which the harvesting structure is in the form of circular cylindrical shell can be simply supported and subjected to base excitation. In this case the harvesting structure is laminated with patches of piezoelectric material.

Analytical and numerical simulations have been developed [19] and experimentally validated the energy harvester from broadband random excitation. For analytical approach, distributed-parameter electro-elastic modelling is employed. For numerical approach, Fourier

series representation of base excitation and Euler-Maruyama scheme to solve ordinary differential equation are used. A method for analysis of piezoelectric energy harvester subjected to random base excitation is proposed [20]. The method is based on probabilistic framework. The base excitation is simulated by amplitude modulated and white Gaussian noise. Energy harvester exposed to random vibrations is developed [21] where the energy harvester has two parts (a) electrical circuit and (b) mechanical single degree of freedom system. Both are coupled through a piezoelectric element. The electrical system consists of resistance and capacitance. The mechanical system consists of linear viscoelastic model. The base excitation is a stationary white noise Gaussian process. The response of the system in terms of mean value of electric power and covariance matrix of system parameters is determined by covariance approach method.

2.5. Latest trends in vibration energy harvesting

Vibration energy from ambient acoustic source is converted into electrical power by cantilever piezoelectric bimorph. In the study by Hu *et al.* [22], the power density of the harvester is characterized by three non-dimensional parameters i.e. the non-dimensional end mass of the harvesting structure, the non-dimensional aspect ratio (length/thickness) and the non-dimensional inductance of the storage circuit. The analyses reveals that the power density can be optimized by two ways i.e. by varying the inductance for each fixed aspect ratio with a fixed end mass; and by choosing an aspect ratio and the end mass with fixed inductance such that the harvesting structure resonates at the frequency of ambient acoustic source. The output voltage with respect to mechanical excitation is improved with the harvesting system configured with piezoelectric beam coupled with magnets. This forms the bi-stable system in response to random vibration. Ferrari *et al.* [23] studied nonlinear converters realized by screen printing low-curing-temperature PZT films on steel cantilevers such that resonant condition is maintained with random excitation. The working frequency of a conventional magnetostrictive cantilever vibration harvester is often higher than ambient vibration frequency.

Dai *et al.* [24] proposed a bi-stable iron-gallium alloy vibration harvester with displacement amplification mechanism. This harvester is tuned to suit the ambient vibration. Wang *et al.* [25] investigated the nanowires as building blocks of nano-generators and applied for harvesting mechanical energy from high frequency acoustic waves and low frequency vibrations for recovering energy from respiration by using piezoelectric polymer thin films.

Shen *et al.* [26] presented a self-powered vibration damping technique that does not just dissipate energy but harvest the energy from the vibrations and supply the power to electronic systems. Liu *et al.* [27] proposed two piezoelectric energy harvesting system based on micro-electro-mechanical systems (MEMS). These harvesting systems can operate with frequency range of wideband operation and is capable of converting low frequency and random vibrations to high frequency oscillations. The first one is incorporated with high resonant frequency cantilever and the second one is added with straight cantilever that makes the low frequency vibration further downward and the voltage and power are improved. Chen *et al.* [28] analyzed broadband characteristics of one dimensional phononic piezoelectric cantilever beams. This is done for widening the resonant bandwidth of energy harvester and is based on phonic band gaps and the vibration band gap. The current studies were focused only on applications in self-powered wireless sensors and low-power electronics. Zuo *et al.* [29] provided a comprehensive review on the large-scale vibration energy harvesting from long bridges, tall buildings, vehicle systems and ocean waves.

2.6. Research gaps

The following research gaps were identified from existing literature on vibration energy harvesting under harmonic and random vibrations.

- Behavior of energy harvester under the influence of random vibration of different frequency bandwidth is not well understood.
- Characterization of energy harvester for maximum power output when subjected to random vibration is not available.
- Relative performance of an energy harvester under the influence of harmonic and random excitations is not clear.

3

Formulations for Vibration Energy Harvesting

3.1. Introduction to cantilever energy harvester

The vibration energy harvesting from both unimorph and bimorph cantilever beams as shown in Figure 3.1 are formulated here to quantify the energy that can be harvested from both harmonic and random vibrations. Erturk *et al.* [30] explained the derivation of piezoelectric energy harvested when subjected to vibrations. The beam in harvester is subjected to a base excitation in terms of force $g(t)$ and moment $h(t)$, which causes the beam to vibrate, inducing an alternating voltage.

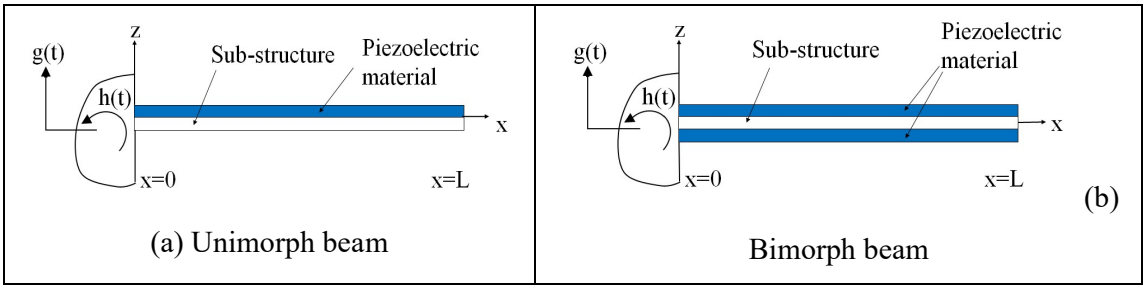

Figure 3.1. Schematic diagram of cantilever piezoelectric power generators

The charge and then voltage generated by the piezoelectric material can be used to power a device directly or to charge a rechargeable battery. In the case of a unimorph cantilever beam, a layer of piezoelectric element is glued to a metallic layer, whereas in a bimorph configuration, a metallic layer is sandwiched between two piezoelectric material layers. In both the cases, a tip mass is attached at the free end to increase the strain as well as tune the natural frequency of structure according to base excitation.

3.2. Assumptions

- The length of the cantilever energy harvester (i.e. the beam) is more relative to its depth and width. Thus, the stresses developed through the depth and width are negligible compared to the longitudinal normal stresses.
- The beam cross section is constant along its length.
- The beam is symmetrical about the lateral axes, resulting in no twisting and torsion.
- Deformations are small.
- The material follows Hooke's law.
- Plane sections remain plane before and after loading i.e. exciation.
- A rigid bond behaviour is assumed between the original beam and PZT substrate.

3.3. Governing equations

The energy harvester studied here is based on a cantilever beam configuration as explained in Figure 3.1. The beam resembles a composite structure (of perfectly bonded isotropic) and follows Euler- Bernoulli beam assumptions. In order to quantify the power output and voltage generated from cantilever energy harvester subjected to a base vibration, the cantilevered beam is depicted as a symmetric bimorph with three layers consisting of a metallic substructure sandwiched between piezoelectric layers.

Let the transverse displacement of beam at an arbitrary point x and at time t along the neutral axis be denoted by $w(x, t)$. The equation of motion for free vibration in the fixed frame of reference if the beam is assumed undamped, can be written as

$$EI\frac{\partial^4 w(x,t)}{\partial x^4}+m\frac{\partial^2 w(x,t)}{\partial t^2}=0 \tag{1}$$

with the following boundary conditions

$$w(x,t)\big|_{x=0} = 0 \quad \text{and} \quad \frac{\partial w(x,t)}{\partial x}\big|_{x=0} = 0 \tag{2a}$$

$$EI\frac{\partial^2 w(x,t)}{\partial x^2}\Big|_{x=L} = 0 \quad \text{and} \quad EI\frac{\partial^3 w(x,t)}{\partial x^3}\Big|_{x=L} = 0 \tag{2b}$$

where EI = bending stiffness in terms of the elastic modulus E and the second moment of area of the cross section I of the layers; m = mass per unit length of the beam; and L = length of the beam.

From [31], the absolute transverse displacement of the beam (i.e. the transverse displacement relative to the fixed reference frame) can be written as

$$w(x,t) = w_b(x,t) + w_{rel}(x,t) \tag{3}$$

where $w_{\text{rel}}(x,t)$ is the transverse tip displacement of beam relative to the clamped end of the beam and $w_{\text{b}}(x,t)$ is the base displacement given by

$$w_b(x,t) = \delta_1(x)g(t) + \delta_2(x)h(t) \tag{4}$$

wherein $\delta_1(x)$ and $\delta_2(x)$ are the displacement influence functions for the transverse base displacement g(t) and small base rotation h(t) of the beam, respectively and $g(t) = W_0 e^{j\omega t}$; $h(t) = \theta_0 e^{j\omega t}$. For the cantilever beam, $\delta_1(x) = 1$ and $\delta_2(x) = 1$. Substituting Eq. (3) into Eq. (1), we get

$$\frac{\partial^4 w(x,t)}{\partial x^4} + m\frac{\partial^2 w_{rel}(x,t)}{\partial t^2} = -m\frac{\partial^2 w_b(x,t)}{\partial t^2} \tag{5}$$

The boundary conditions are:

$$w_{rel}(x,t)\big|_{x=0} = 0 \quad \text{and} \quad \frac{\partial w_{rel}(x,t)}{\partial x}\big|_{x=0} = 0 \tag{6a}$$

$$EI\frac{\partial^2 w_{rel}(x,t)}{\partial x^2}\Big|_{x=L} = 0 \quad \text{and} \quad EI\frac{\partial^3 w_{rel}(x,t)}{\partial x^3}\Big|_{x=L} = 0 \tag{6b}$$

3.4. Solutions under harmonic excitation

The solution of Eq. (5) considering the two boundary conditions in Eq. (6) can be represented as a convergent series of Eigen functions. The method of separation of variables is used to solve Eq. (5) by separating the spatial and temporal functions as

$$w_{rel}(x,t) = \sum_{r=1}^{\infty} \phi(x)\eta(t) \tag{7}$$

Substituting Eq. (7) into Eq. (5) gives

$$\frac{EI}{m}\frac{1}{\phi(x)}\frac{d^4\phi(x)}{dx^4} = -\frac{1}{\eta(t)}\frac{d^2\eta}{dt^2} \tag{8}$$

The left hand side of Eq. (8) is dependent on x while right hand side depends on t and both are independent variables. According to the method of separation of variables both sides of equation must be equal to the same constant γ.

Therefore,

$$\frac{EI}{m}\frac{1}{\phi(x)}\frac{d^4\phi(x)}{dx^4} = -\frac{1}{\eta(t)}\frac{d^2\eta}{dt^2} = \gamma \tag{9}$$

which gives

$$\frac{d^4\phi(x)}{dx^4} - \gamma\frac{m}{EI}\phi(x) = 0 \tag{10a}$$

$$\frac{d^{42}\eta(t)}{dt^2} + \gamma\eta(t) = 0 \tag{10b}$$

Let $\gamma = \omega^2$, then the solution forms of Eqs (10a) and (10b) will be

$$\phi(x) = A\cos\left(\frac{\lambda}{L}x\right) + B\cosh\left(\frac{\lambda}{L}x\right) + C\sin\left(\frac{\lambda}{L}x\right) + D\sinh\left(\frac{\lambda}{L}x\right) \tag{11a}$$

$$\eta(t) = E\cos(\omega t) + F\sin(\omega t) \tag{11b}$$

where,

$$\lambda^4 = \omega^2\frac{mL^4}{EI} \tag{11c}$$

in which ω is the natural circular frequency and A, B, C,D, E, and F are unknown constants. Applying the boundary conditions mentioned in Eq. (6) and solving the Eigen value problem

in Eqs (11a-b) considering that the Eigen value of the r^{th} vibration mode is λ_r and the r^{th} Eigen function is $\Phi_r(x)$, we get,

$$\phi_r(x) = A_r\left[\cos\left(\frac{\lambda_r}{L}x\right) - \cosh\left(\frac{\lambda_r}{L}x\right) + \varsigma_r\left(\sin\left(\frac{\lambda_r}{L}x\right) + \sinh\left(\frac{\lambda_r}{L}x\right)\right)\right] \tag{12}$$

where,

$$\varsigma_r = \frac{\sin\lambda_r - \sinh\lambda_r}{\cos\lambda_r + \cos\lambda_r};\ \lambda_r^2 = \omega_r\sqrt{\frac{mL^4}{EI}};\ \text{and}\ \omega_r = 2\pi f_r \tag{13}$$

in which f_r is r^{th} natural frequency. The mass normalized form of Eigen functions $\phi_r(x)$ satisfies the orthogonality conditions. Using Eq. (5) with boundary conditions in Eq. (6a-b) and orthogonality conditions, the partial differential equation of motion can be reduced to an infinite set of ordinary differential equation of the form

$$\frac{d^2\eta_r}{dt^2} + 2\zeta\omega_r\frac{d\eta_r(t)}{dt} + \omega_r^2\eta_r(t) - \tilde{\theta}_r V(t) = F_r(t) \tag{14}$$

where, η_r = modal parameter, $V(t)$ = voltage, ζ_r = damping factor, ω_r = natural frequency, $F_r(t)$ is the forcing function given as

$$F_r(t) = \omega^2 W_0\left(m\int_0^L \phi_r(x)dx + M_t\phi_r(L)\right) + \omega^2\theta_0\left(\int_0^L x\phi_r(x)dx + M_t L\phi_r(L)\right) \tag{15}$$

and θ_r is the modal electro-mechanical coupling parameter which is given by

$$\theta_r = \begin{cases} e_{31}bh_{pc}\left.\frac{d\emptyset_r(x)}{dx}\right|_{x=L} \\ 2e_{31}bh_{pc}\left.\frac{d\emptyset_r}{dx}\right|_{x=L} \end{cases} \text{for series and parallel connections, respectively.} \tag{16}$$

Here, b is the width of the beam and $h_{pc} = 0.5(h_p+h_s)$ where, h_p is thickness of piezoelectric layer and h_s is the thickness of the substructure. The only source of mechanical strain is the axial strain in piezoelectric material due to bending of harvesting structure. For the given electrode configuration, the tensorial representation of piezoelectric constitutive equation is given by

$$D_3 = e_{31}S_1 + \varepsilon_{33}^S E_3 \tag{17}$$

where, D_3 is the electric displacement component, e_{31} is the piezoelectric stress constant, S_1 is the elastic compliance at constant electric field, ε_{33}^s is the permittivity component at constant strain, and E_3 is the electric field in the direction of thickness. As the external circuit admittance

across the electrodes is $1/R$ where R is the load resistance, the electric current output can be obtained from Gauss' law as

$$\frac{d}{dt}\left(\int D.ndA\right)=\frac{V(t)}{R} \tag{18}$$

where, D is the electric displacement and n is the unit outward normal; and integration is done over electrode area A.

Substituting D and electric field $E_3 = -V(t)/h_p$ into Eq. (17) and Eq. (18), we get,

$$C_p^{eq}\frac{dV(t)}{dt}+\frac{V(t)}{R_l}+\sum_{r=1}^{\infty}\tilde{\theta}_r\frac{d\eta_r(t)}{dt}=0 \tag{19}$$

where, $C_p^{eq}=\dfrac{\varepsilon_{33}^S bl}{h_p}$ = internal capacitance.

Voltage $V(t)$ can be obtained by solving the Eqs (14) and (19), as given below.

$$V(t)=\frac{\sum_{r=1}^{\infty}\dfrac{-j\omega\tilde{\theta}_r F_r}{\omega_r^2-\omega^2+j2\zeta_r\omega_r\omega}}{\dfrac{1}{R}+j\omega C_p^{eq}+\sum_{r=1}^{\infty}\dfrac{j\omega\tilde{\theta}_r^{\,2}}{\omega_r^2-\omega^2+j2\zeta_r\omega_r\omega}} \tag{20}$$

and the power output is given as

$$P=\frac{V(t)}{R}\quad . \tag{21}$$

3.5. Solutions under random excitations

Let us consider the random base excitation to be Gaussian white noise signal. The Gaussian white noise signal has a constant amplitude of power spectral density (PSD) of 'S_0' throughout the frequency bandwidth. The analytical solution for the expected (mean) power can be derived using this property of the excitation along with the voltage frequency response function (FRF) derived in the previous section. Further, V(t) can be written as

$$\alpha(\omega)\left(-\omega^2 W_0 e^{j\omega t}\right)+\mu(\omega)\left(-\omega^2\theta_0 e^{j\omega t}\right) \tag{22}$$

where voltage output – to – translation base acceleration FRF is given as

$$\alpha(\omega)=\frac{\sum_{r=1}^{\infty}\frac{-j\omega\tilde{\theta}_r\sigma_r}{\omega_r^2-\omega^2+j2\zeta_r\omega_r\omega}}{\frac{1}{R}+j\omega C_p^{eq}+\sum_{r=1}^{\infty}\frac{j\omega\tilde{\theta}_r^2}{\omega_r^2-\omega^2+j2\zeta_r\omega_r\omega}} \tag{23}$$

and voltage output – to – rotational base acceleration FRF is given as

$$\mu(\omega)=\frac{\sum_{r=1}^{\infty}\frac{-j\omega\tilde{\theta}_r\tau_r}{\omega_r^2-\omega^2+j2\zeta_r\omega_r\omega}}{\frac{1}{R}+j\omega C_p^{eq}+\sum_{r=1}^{\infty}\frac{j\omega\tilde{\theta}_r^2}{\omega_r^2-\omega^2+j2\zeta_r\omega_r\omega}}\ . \tag{24}$$

If the base is assumed to be not rotating i.e. $h(t)$=0 and $\theta_0 = 0$ in equation (22), but translating with $g(t)=W_0e^{j\omega t}$, the voltage in Eq. (22) becomes $\alpha(\omega)(-\omega^2W_0e^{j\omega t})$ and modal mechanical forcing function becomes $F_r=-\sigma_r\omega^2W_0$.

We know that the electrical power output is $\frac{V^2(t)}{R}$ then the expected value of the power output is

$$E[P(t)]=\int_{-\infty}^{\infty}\frac{S_0}{R}|\alpha(\omega)|^2\,d\omega \tag{25}$$

Therefore, the analytical solution for the expected power output is

$$E[P(t)]=\int_{-\infty}^{\infty}\frac{S_0}{R}\left|\frac{\sum_{r=1}^{\infty}\frac{-j\omega R\theta_1\sigma_1}{\omega_r^2-\omega^2+j2\zeta\omega_1\omega}}{\frac{1}{R}+j\omega C_p^{eq}+\sum_{r=1}^{\infty}\frac{-j\omega R\theta_1\sigma_1}{\omega_r^2-\omega^2+j2\zeta_r\omega_r\omega}}\right|^2 d\omega \tag{26}$$

which is the exact representation considering the excitation of harvester in the entire frequency bandwidth. The analytical solution of the expected power for the fundamental vibration mode is estimated from

$$E[P(t)]\cong E\left[\hat{P}(t)\right]=\int_{-\infty}^{\infty}\frac{S_0}{R}\left|\hat{\alpha}(\omega)\right|^2 d\omega \tag{27}$$

where, α(ω) is voltage output- base acceleration single mode FRF and is given as

$$\hat{\alpha}(\omega)=\frac{-j\omega R\theta_1\sigma_1}{\left(1+j\omega RC_p^{eq}\right)\left(\omega_1^2-\omega^2+j2\zeta\omega_1\omega\right)+j\omega R\tilde{\theta}_1^2} \tag{28}$$

Substituting Eq. (28) in (27), we get

$$E\left[\hat{P}(t)\right] = \int_{-\infty}^{\infty} \frac{S_0}{R} \left| \frac{-j\omega R \tilde{\theta}_1 \sigma_1}{\left(1 + j\omega R C_p^{eq}\right) + (\omega_1^2 - \omega^2 + j2\zeta\omega_1\omega) + j\omega R \tilde{\theta}_1^2} \right|^2 d\omega \ . \qquad (29)$$

3.6. Summary

In the present chapter, the schematic diagram is explained for unimorph and bimorph cantilever beam for piezoelectric energy harvesting. The voltage across the circuit and power generated during the process is derived by considering Euler-Bernoulli's equation. The derivations are carried out for the beam when it is subjected to simple harmonic motion and random vibrations. Equations (20), (21) derives the voltage across the circuit and power generated in case of harmonic excitation whereas, Equation (26) represents the analytical solution for the expected power output in case of random excitation.

4

Numerical Simulation of Energy Harvester under Harmonic Excitation

4.1. Introduction

The energy harvester analyzed in this study consists of a piezoelectric bimorph with steel substructure clamped at one end of the vibrating source such as a machinery or a vehicle, with a proof mass mounted on its other end as shown in Figure 4.1. In order to establish the finite element analysis (FEA) simulation procedure, COMSOL Multiphysics 5.0 [32] software tool is used.

4.2. Part-1: Characterization of Bimorph CEH and its validation

4.2.1. Geometry and material parameters

The considered cantilever energy harvester (CEH) structure as shown in Figure 4.1 has the dimensions: length = 21 mm, width = 14 mm and thickness = 0.16 mm.

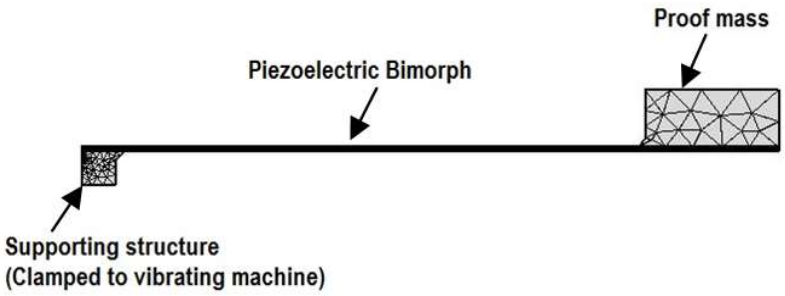

Figure 4.1. Cantilever type energy harvester showing the major components

The structure is made of structural steel of thickness 0.04 mm with Young's modulus E = 200 GPa and Poisson's ratio υ = 0.28. This structure is sandwiched between top and bottom layers of piezo-electric material PZT-5A of thickness 0.06mm. The base of this harvester is mounted on a machine that is vibrating at 1g. The mechanical and physical properties of piezo-electric material PZT-5A used in simulation are taken from [33] and is given in Table 4.1.

Table 4. 1. Properties of PZT-5A

Property	Value	Unit
Density (ρ)	7750	kg/m^3
Elastic compliance matrix (S) $\begin{bmatrix} S_{11} & S_{12} & S_{13} & S_{14} & S_{15} & S_{16} \\ S_{21} & S_{22} & S_{23} & S_{24} & S_{25} & S_{26} \\ S_{31} & S_{32} & S_{33} & S_{34} & S_{35} & S_{36} \\ S_{41} & S_{42} & S_{43} & S_{44} & S_{45} & S_{46} \\ S_{51} & S_{52} & S_{53} & S_{54} & S_{55} & S_{56} \\ S_{61} & S_{62} & S_{63} & S_{64} & S_{65} & S_{66} \end{bmatrix}$	$\begin{bmatrix} 1.6e\text{-}11 & -7.2e\text{-}12 & 1.8e\text{-}11 & 0 & 0 & 0 \\ -7.2e\text{-}12 & -5.7e\text{-}12 & 1.64e\text{-}11 & 0 & 0 & 0 \\ 1.8e\text{-}11 & 1.64e\text{-}11 & -5.7e\text{-}11 & 0 & 0 & 0 \\ 0 & 0 & 0 & 4.7e\text{-}11 & 0 & 0 \\ 0 & 0 & 0 & 0 & 4.7e\text{-}11 & 0 \\ 0 & 0 & 0 & 0 & 0 & 4.4e\text{-}11 \end{bmatrix}$	1/Pa
Coupling matrix (e) $\begin{bmatrix} e_{11} & e_{12} & e_{13} & e_{14} & e_{15} & e_{16} \\ e_{21} & e_{22} & e_{23} & e_{24} & e_{25} & e_{26} \\ e_{31} & e_{32} & e_{33} & e_{34} & e_{35} & e_{36} \end{bmatrix}$	$\begin{bmatrix} 0 & 0 & -5.35 & 0 & 0 & -5.35 \\ 0 & 0 & 15.7 & 0 & 12.3 & 0 \\ 12.3 & 0 & 0 & 0 & 0 & 0 \end{bmatrix}$	C/m^2
Relative permittivity (e) [e_{11} e_{22} e_{33}]	[919.1 919.1 826.6]	

4.2.2. FE model setup

The harvester is discretized in finite element domain with tetrahedral elements having the size range of 0.0063 to 1.41 mm with element growth rate of 1.3.

4.2.3. FEA under harmonic excitations

4.2.3.1. Performance of harvester without a proof mass

The FEA of the energy harvester is carried out with fixed load resistance of R = 12 kΩ and quantified the power output P and voltage V as a function of vibrating frequencies as shown in Figure 4.2. This harvester exhibits maximum power and voltage outputs at the natural frequency of around 218 Hz for the given R.

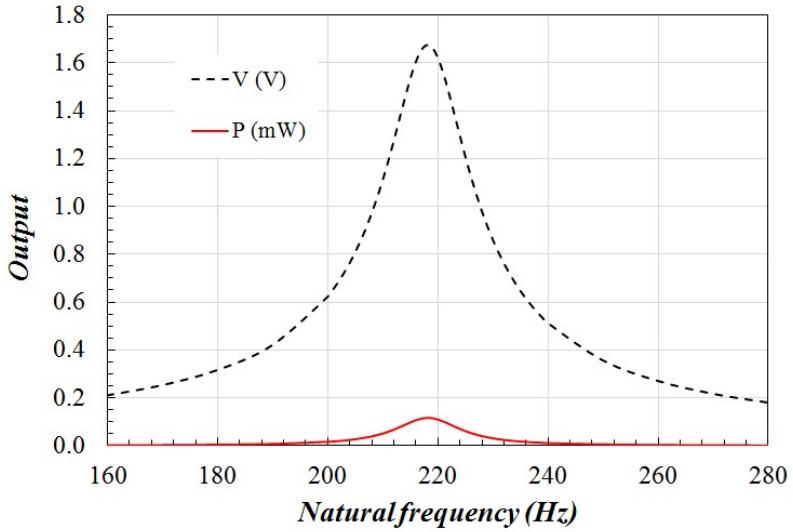

Figure 4.2. Frequency response: power output and voltage

Further, the load resistance R is varied from 100 Ω to 100 kΩ with base excitation matching the natural frequency of the harvester $f_r = 218\ Hz$ and quantified the power output and voltage as a function of electrical load as shown in Figure 4.3. The power output increases with R up to about 12kΩ and afterwards decreases gradually. The voltage increases asymptotically with R and its increase is steep between about 2kΩ and 50 kΩ.

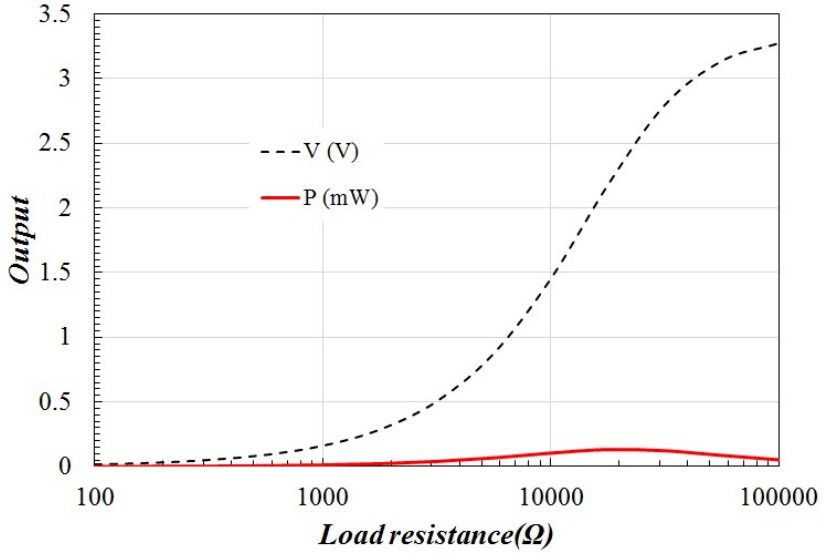

Figure 4.3. Load dependence: power output and voltage

4.2.3.2 Comparison of results

In order to validate the simulation procedure and to extend it for further studies, the simulation is repeated with a proof mass of say 740 mg on harvester. The performance of this basic harvester is shown in Figure 4.4 and is compared with Lefeuvre [33].

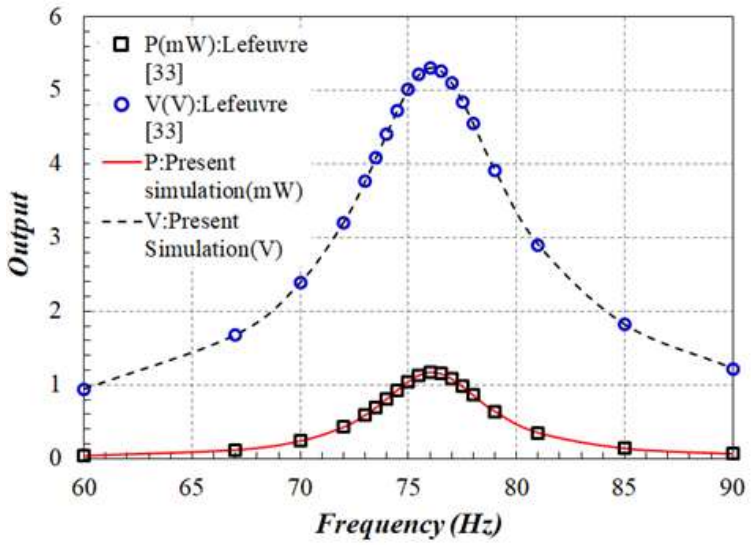

(a) Dependence on excitation frequency

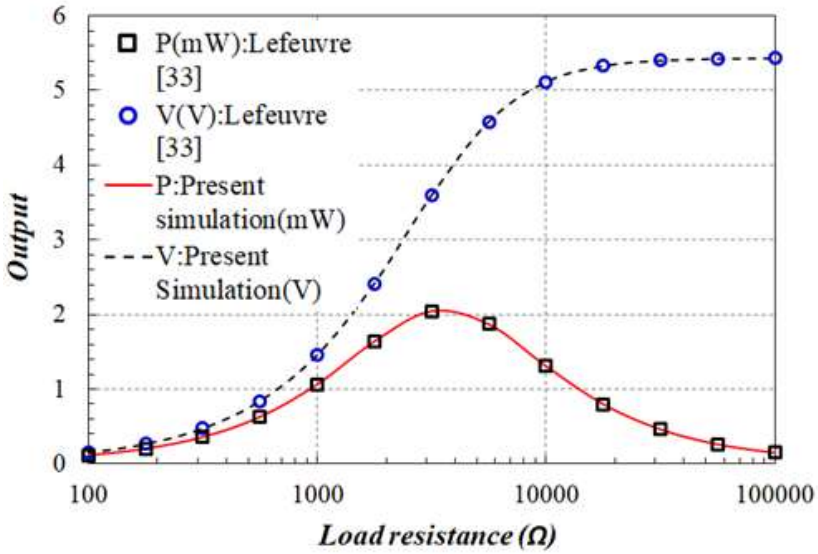

(b) Dependence on load resistance

Figure 4.4. Power and voltage outputs from basic harvester with a proof mass

The power and voltage outputs increase steadily with base excitation, reach their maxima at excitation close to the natural frequency of 76.5 Hz of harvester and afterwards decrease to their initial values. These outputs are symmetrical on both sides of natural frequency excitation as shown in Figure 4.4(a). The load dependence of this harvester outputs shown in Figure 4.4(b) are similar to that in Figure 4.3. However, the generated voltage output increases steadily up to about 20 kΩ and afterwards exhibits constant output irrespective of any increase in load resistance. The maximum power is generated for a load resistance of about 3 kΩ as shown in Figure 4.4(b). The present results from FEA simulation of this basic harvester are compared with the results available in [33] and a perfect agreement is found between them as shown in Figure 4.4.

Thus, the presently validated FEA simulation procedure is used to further characterize the performance of this energy harvester.

4.2.4. Characterization of cantilever energy harvester (CEH) under harmonic excitation

The FEA procedure is extended to characterize the performance of CEH. The harvester is discretized into tetrahedral elements of size ranging between 0.0063 to 1.41 mm with element growth rate of 1.3. The harvesting structure is fixed at one end and subjected to harmonic base excitation. The harmonic analysis is carried out with different magnitudes of harmonic

vibrations, different proof masses and different widths of structure for natural frequency, power and stresses.

4.2.4.1. Characteristics under increasing base accelerations

The characteristics of this energy harvester are analyzed under influence of different loading and geometric conditions and are explained in this section.

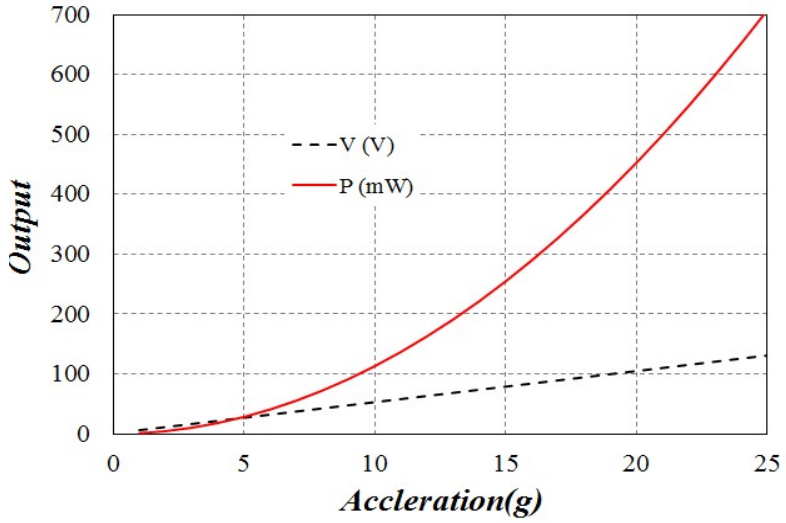

(a) Power and voltage outputs *w.r.t.* base acceleration

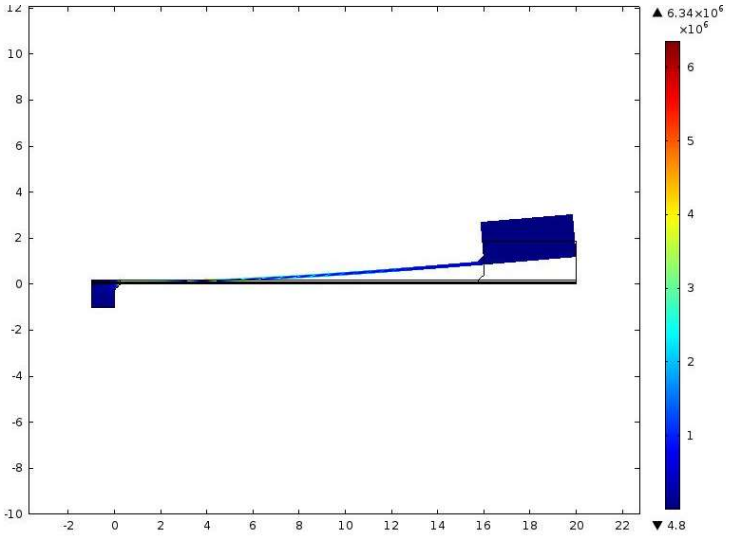

(b) Stress distribution at 25g excitation

Figure 4.5. Effect of base acceleration on basic harvester

The power output and the voltage developed in basic harvester at the resonant frequency of 76.5 Hz is analyzed under different base accelerations ranging from 1g to 25g and the results are shown in Figure 4.5(a). The power output increases almost exponentially from minimum

to a maximum of 700 mW as the base acceleration increase from 1g to 25g whereas the voltage generated increases almost linearly and reaches about 130V at 25g. The von-Mises stress (Pa) distribution in harvester is shown in Figure 4.5(b) at a base acceleration of 25g.

4.2.4.2. Effect of proof mass and width of beam on natural frequency of basic harvester

The maximum power output occurs when excitation matches the natural frequency of the structure as evidenced in the aforementioned studies. The natural frequency of any structure depends on its mass and stiffness and hence the characteristic studies are carried out to quantify the natural frequency and power output with the variation of proof mass M_t at tip and width of the beam. The harvester is analyzed by varying the proof mass from 0 to 1000 mg and the beam width from 10 to 20 mm. The results are shown in Figure 4.6. As the proof mass is varied from 0 to 1000 mg, the natural frequency monotonically follows the decreasing trend irrespective of the beam width. It is also observed that the natural frequency of structure with a particular proof mass is lower for a lower beam width and higher for higher beam width. Whereas, the power output of the structure with proof mass from 0 to 200 mg increases with increase in width and after 200 mg the power output increases with decrease in width.

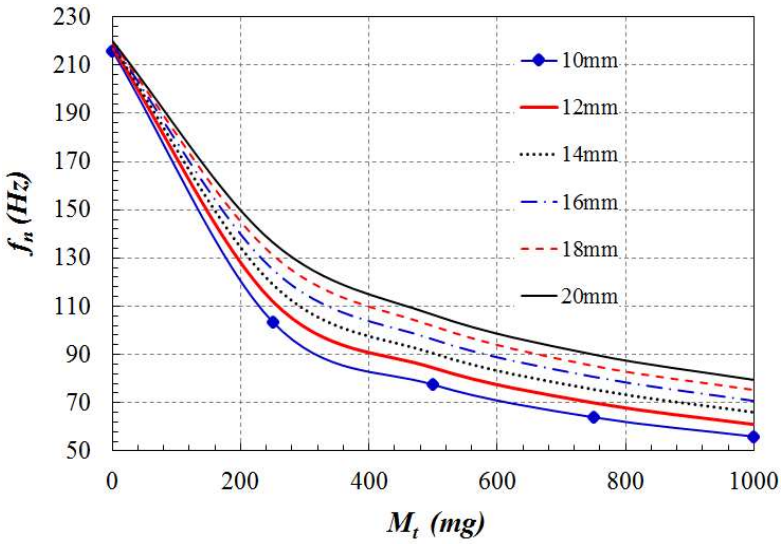

(a) Natural frequency *w.r.t* proof mass and beam width

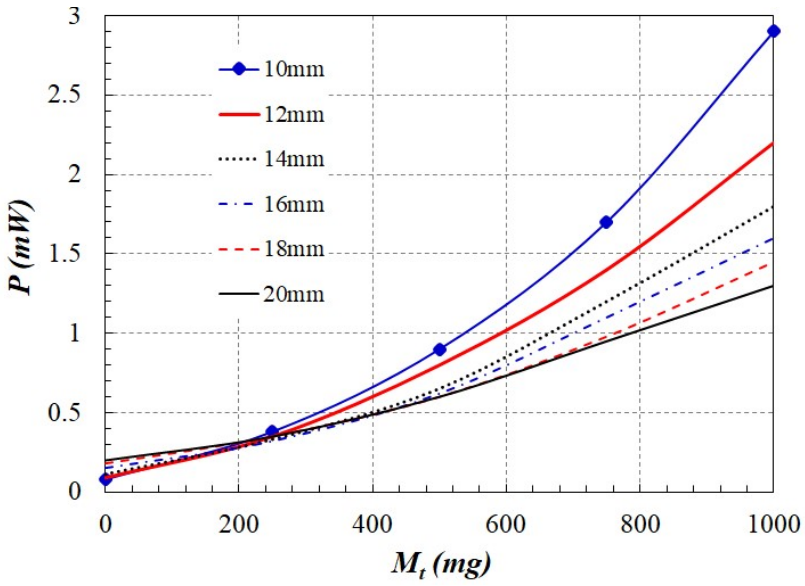

(b) Power output *w.r.t* proof mass and beam width

Figure 4.6. Natural frequency and power output of the structure as a function of proof mass and beam width

Different studies were carried out for quantifying the power output and voltage from cantilever energy harvester by varying the proof mass and beam width when exposed to a simple harmonic motion under 1g acceleration. In all these studies, it is essential to see that the induced stresses in the beam substrate and PZT layers and the interfacial stresses between the interfaces must be within the permissible limits. They are analyzed in this section.

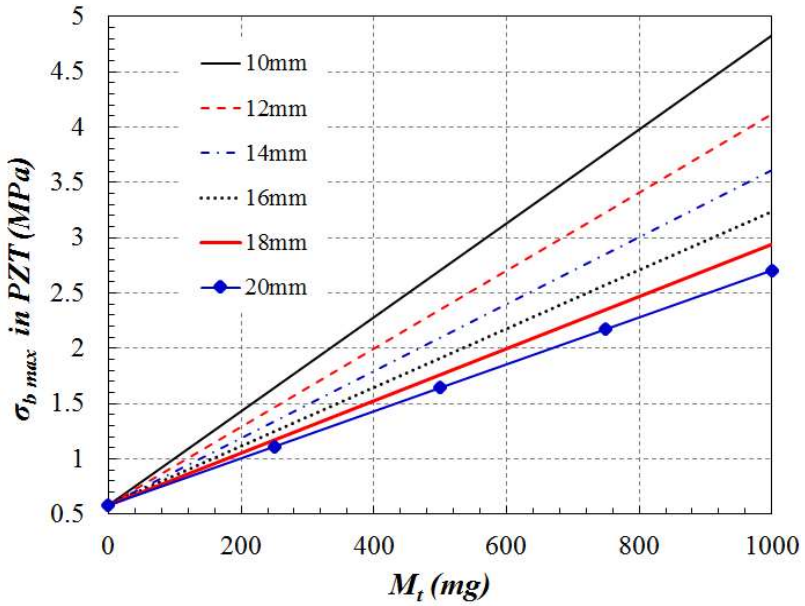

(a) Maximum bending stress in PZT-5A *w.r.t* proof mass and beam width

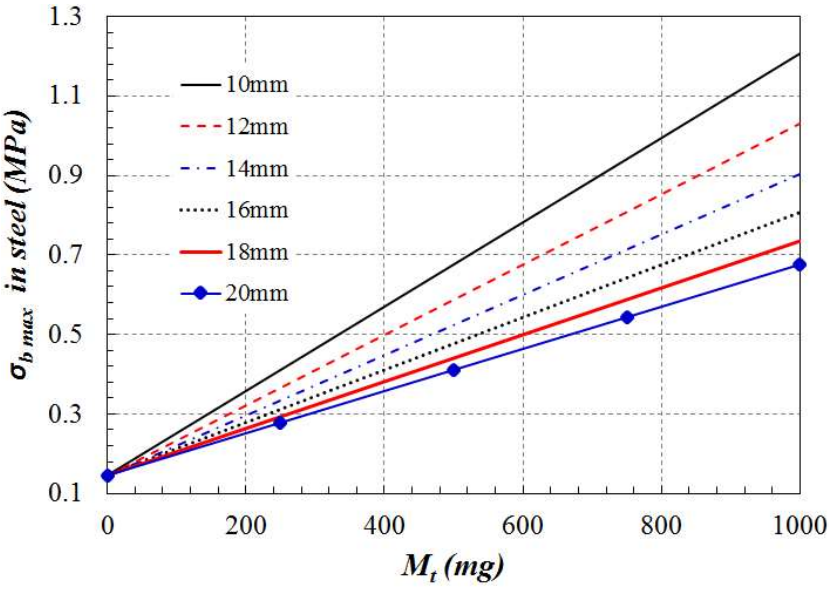

(b) Maximum bending stress in steel substructure *w.r.t* proof mass and beam width

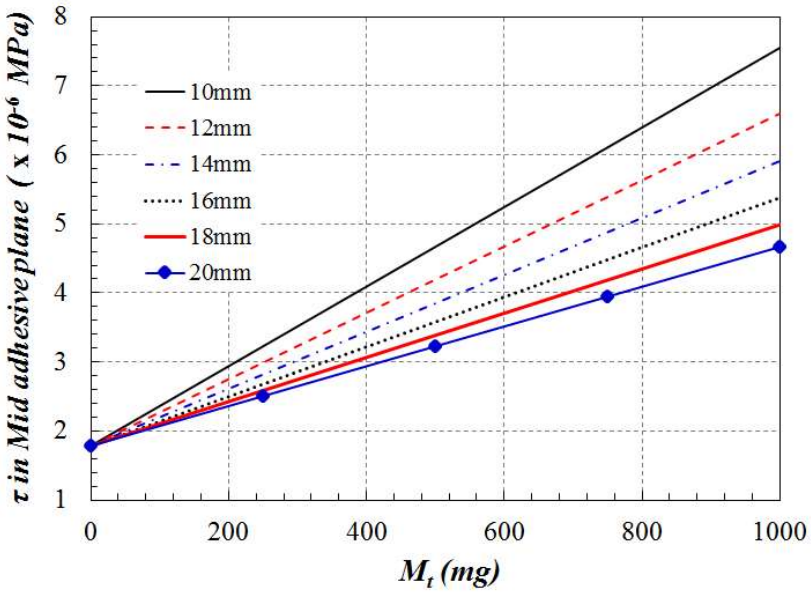

(c) Shear stress in mid-adhesive layer *w.r.t.* proof mass and beam width

Figure 4.7. Stresses induced in harvesting structure *w.r.t.* proof mass and beam width

The stresses that are predominant are bending stresses (σ_b) in PZT-5A layer and structural steel, and shear stress (τ) in mid-adhesive plane. Euler-Bernoulli beam theory is used for calculating maximum bending stress. The results are shown in Figure 4.7. The stresses are increasing linearly with respect to increase in proof mass and reduction in beam width. For a given proof mass, the maximum bending stress is induced in the structure having lesser beam width. From Figures 4.7(a-b), the maximum bending stress in PZT and steel substructure of harvesting structure with beam width of 10 mm and proof mass of 1000 mg are 4.8 MPa and 2.0 MPa, respectively. It is to be noted that the PZT-5A patches are glued to the steel substructure by adhesives. These adhesives are weak in shear. Shear stress in mid-adhesive plane is calculated for harvesting structure with different proof mass and beam width. Figure 8(c) shows that the shear stress in mid-adhesive plane is increasing linearly with respect to proof mass and reduction in beam width. The maximum shear stress in mid-adhesive layer is found in the harvesting structure for a beam width of 10 mm with a proof mass of 1000 mg. The maximum bending stress in PZT-5A and steel as well as shear stress in adhesives are compared with respective yield strengths. The average value of modulus of rupture (MOR) for PZT-5A as 81.8 MPa [34]. The allowable strength for steel substructure is 240 MPa and shear strength of adhesive is 12 MPa. The induced stresses are all well within these allowable limits and hence, the structure is safe under the present loading conditions thus analyzed.

4.2.4.3 Studies on energy harvester with beam width of 10 mm

Based on the characteristic studies thus conducted and discussed above, it is found that the cantilever energy harvester with a beam width of 10 mm generates maximum power of 0.08 mW, 0.38 mW, 0.9 mW, 1.05 mW, 1.7 mW and 2.9 mW when attached respectively with proof masses of 0 mg, 250 mg, 500 mg, 750 mg and 1000 mg when excited at its natural frequencies of 216 Hz, 103.5 Hz, 77.5 Hz, 75 Hz, 64 Hz and 56 Hz, respectively. These are the observations when the harvester is exposed to 1g base acceleration. Therefore, further studies are done to obtain the response of the harvester having a beam width of 10 mm and again with a proof mass varying from 0 to 1000 mg. The harvester is subjected to a base acceleration starting from 1g to 30g. The results are shown in Figure 4.8. Figure 4.8(a) indicates that there is a limitation on the subjected base acceleration on this beam for higher proof mass at tip. The limitation comes from the MOR of PZT-5A which is at 81.8 MPa, which means that the bending stress in PZT-5A, a part of beam along with any proof mass and exposed to base acceleration should not exceed 81.8 MPa. The feasible options for maximum power output and voltage within the limits of MOR of PZT-5A are summarized in Table 4.2 based on the response shown in Figure 4.8(a).

Table 4. 2. Feasible options for maximum power output and voltage

Option No.	Proof mass (mg)	Base acceleration (g)
1	0 - 1000	1 - 15
2	0 - 750	20
3	0 - 500	25 - 30

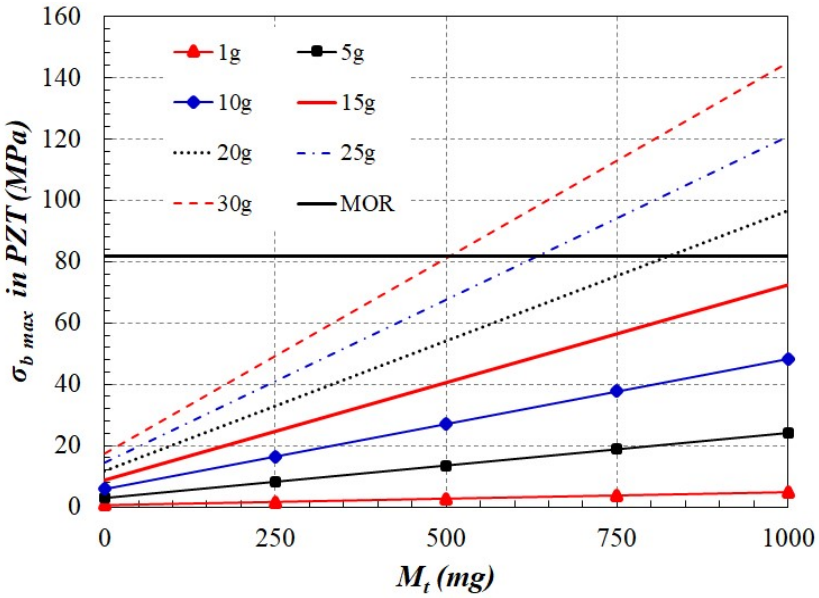

(a) Maximum bending stress in PZT-5A *w.r.t* proof mass and base acceleration

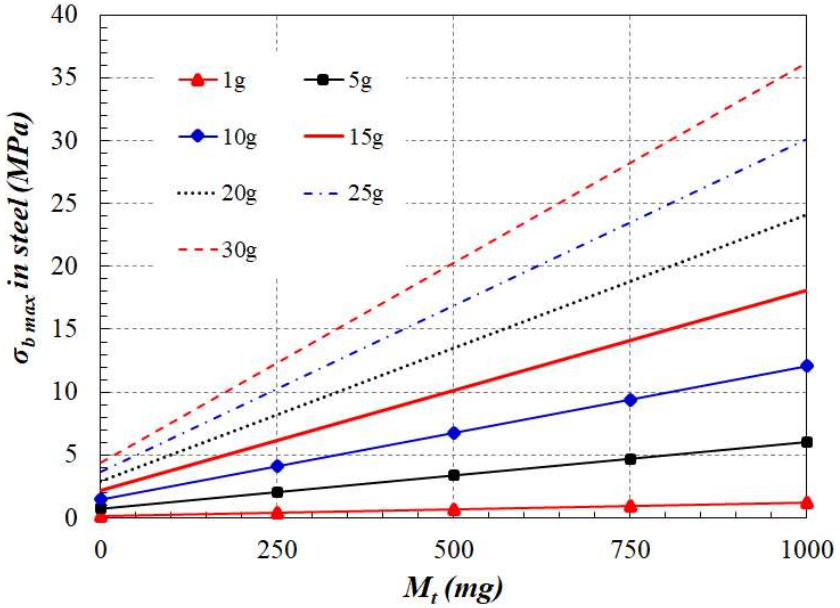

(b) Maximum bending stress in steel *w.r.t* proof mass and base acceleration

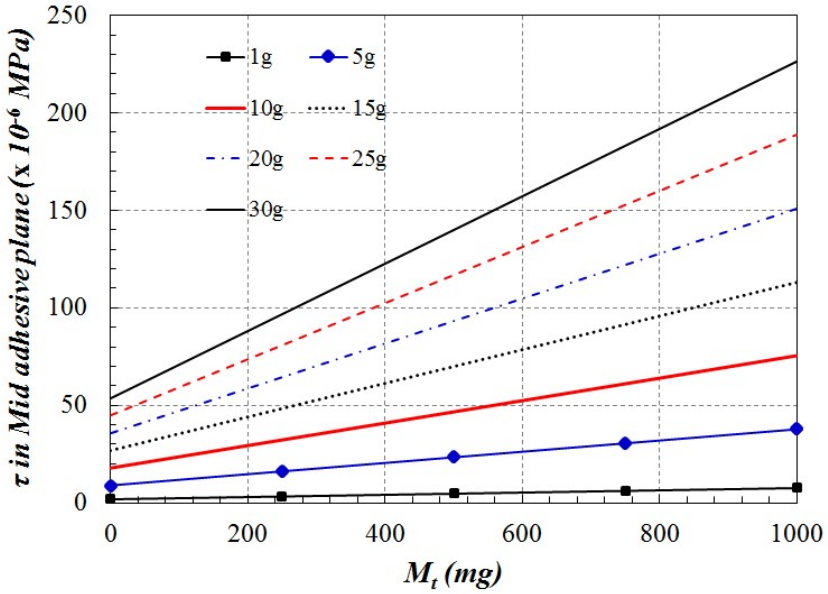

(c) Shear stress in mid-adhesive plane *w.r.t* proof mass and base acceleration

Figure 4.8. Stresses induced in harvesting structure of 10 mm beam width w.r.t proof mass and base acceleration

Except the above limitation on the induced bending stresses in the PZT layer, the stresses are well below the permissible limits in steel substructure and the adhesive layer as shown in Figures 4.8(b-c). Based on the feasible options of proof mass and base acceleration mentioned

in Table 2, the power output and voltage generated by energy harvester is quantified and shown respectively in Figures 4.9(a-b).

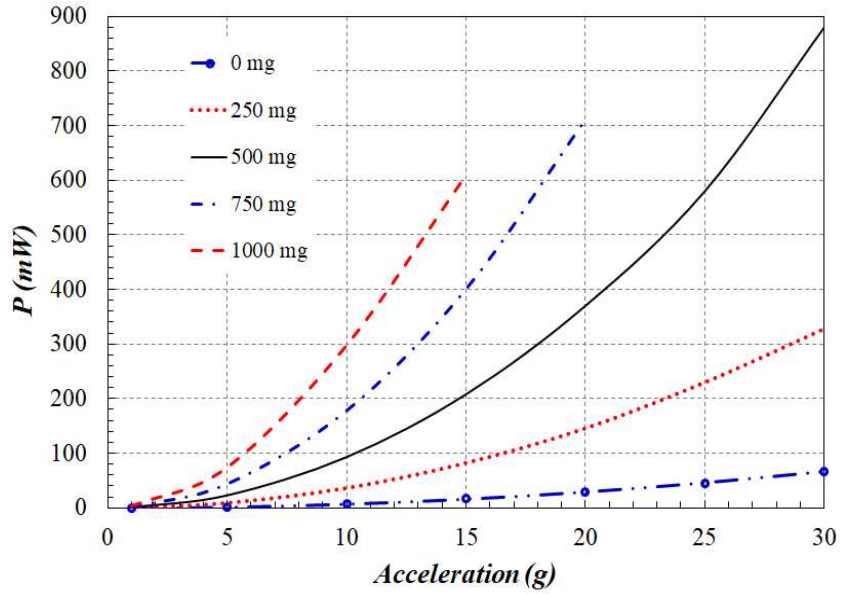

(a) Power output with different proof masses *w.r.t* base acceleration

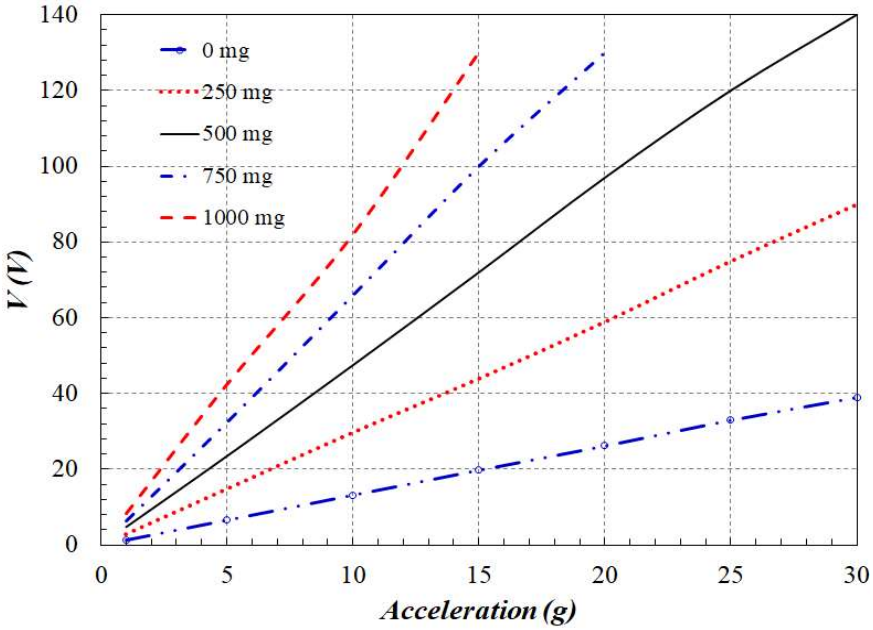

(b) Voltage developed in harvester with different proof masses *w.r.t* base acceleration

Figure 4.9. Feasible outputs from cantilever energy harvester based on proof mass and base acceleration

These characteristic studies show that the cantilever energy harvester with a proof mass of 500 mg when subjected to a base acceleration of 30 g, generates the maximum power output of 880 mW at a maximum voltage of 140 V as evidenced from Figure 4.9.

4.3. Part-2: Characterization of Unimorph CEH

The studies on CEH performed and mentioned in the previous sections gave sufficient understanding on performance of harvesting structure under harmonic excitation and procedure for carrying out the finite element analysis as well. During these studies, the reference for geometry and material is taken from literature in which the harvesting structure and piezoelectric material are so that they are not physically available in the market. In order to carry out experimental investigations for validation of numerical results, the numerical simulation of such a geometry and material is executed which is readily available in market.

4.3.1. Geometry and material properties

The CEH consists of a piezoelectric unimorph. The piezoelectric material used in present study is a semi-crystalline PVDF (Polyvinylidene fluoride), LTD4-28K/L of 40 μm thickness and bonded over an aluminium alloy AA2014 base cantilever beam of dimensions 171x22x2 mm as shown in Figure 4.10(a) in which the geometry of the harvesting structure with piezoelectric layer is shown in red color and aluminum substrate in grey color. A ϕ6 mm hole is provided at the fixed end of this harvester for clamping with the base exciting structure. The piezoelectric material is bonded to the aluminium substructure by cyanoacrylate adhesive Mbond 200. The actual configuration of the harvester is shown in Figure 4.10(b). The properties of PVDF taken from manufacturer's data sheet are given in Table 4.3 which are used as inputs in FEA simulations.

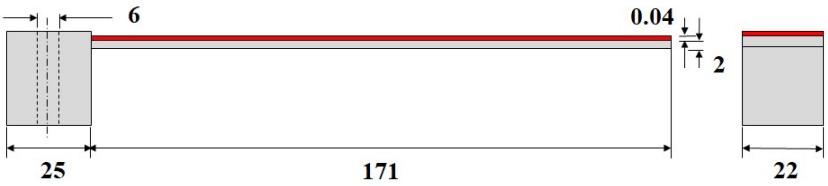

(a) Geometry of cantilever energy harvester (all dimensions in mm)

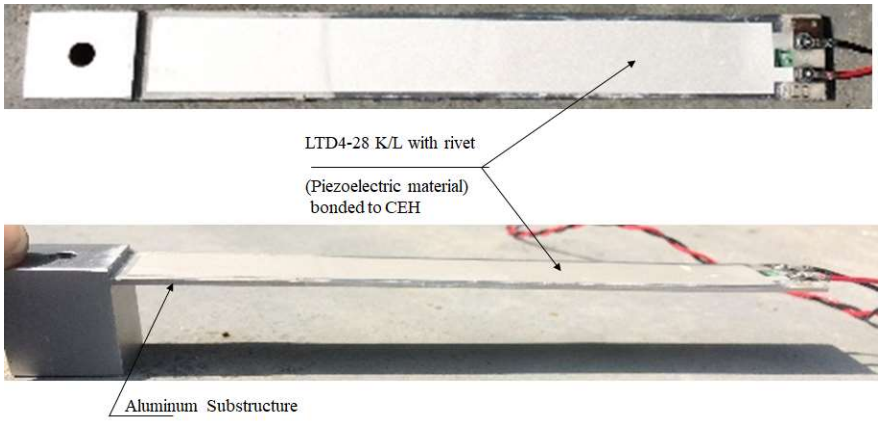

(b) Physical configuration

Figure 4.10. Unimorph cantilever energy harvester

Table 4. 3. Properties of PVDF

S. No.	Property	Value	Unit
1	Density	1780	kg/m^3
2	Piezoelectric strain constant (d_{31})	23 x 10^{-12}	C/N
3	Piezoelectric strain constant (d_{33})	-33 x 10^{-12}	C/N
4	Piezoelectric stress constant (g_{31})	216 x 10^{-3}	Vm/N
5	Piezoelectric stress constant (g_{33})	-330 x 10^{-3}	Vm/N
6	Electromechanical coupling factor (k_{31})	12.0%	-
7	Electromechanical coupling factor (k_t)	14.0%	-
8	Young's modulus of elasticity (E)	4.0	GPa
9	Capacitance (C)	11.0	nF

4.3.2. FEA model setup

A simplified geometric model of CEH as shown in Figure 4.11(a) is modeled in ANSYS 18.1 Workbench Space claim [35]. The FEA model with piezoelectric material properties is prepared in *PiezoAndMEMS* extension module. This model is made up of three parts a) aluminum alloy base structure, b) piezoelectric material i.e. PVDF, and c) resistor. The PVDF is attached to the aluminum substructure using a bonded connection i.e. a rigid bond behavior. All three components of CEH are discretized for FEA. Aluminum alloy substructure is discretized by 356 elements and PVDF by 60 elements. Both are discretized by 20 node tetrahedron elements having translational nodal degrees of freedom in *x*, *y* and *z* directions. The CIRCU 94 element is chosen to simulate basic linear electric circuit components that can be

directly connected to the piezoelectric FEA domain. Since resistor is being used as load, the *keyopt* (1) = 0 with resistance 102 kΩ is chosen. This resistor component is one dimensional and discretized with single 1D element which has two nodes, each node having voltage as the degree of freedom.

The meshed FE model of the CEH with boundary conditions is shown in Figure 4.11(b). The material properties for piezoelectric material, aluminum alloy substructure, and resistor are assigned for the FEA model as per the values provided in Tables 4.2 and 4.3. Polystyrene material available in database [36] is assigned to the resistor with a resistance value of 102 kΩ. The voltage degree of freedom at nodes 1 and 2 of resistor are coupled with the terminals of PVDF.

Table 4. 4. Properties of aluminum alloy AA2014 material

S. No.	Properties	Value
1	Density (kg/m^3)	2650
2	Modulus of elasticity (MPa)	70000
3	Poisson's ratio	0.3

4.3.3. Numerical simulation under 1g with different load resistances

Initially, in the first stage, modal analysis was carried out for the CEH considering a damping coefficient of 0.02, as shown in Figure 4.11(a-b) and predicted a fundamental natural frequency of 27.5 Hz as shown in Figure 4.11(c).

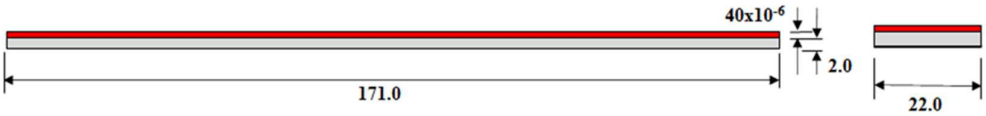

a) Geometry of FEA model

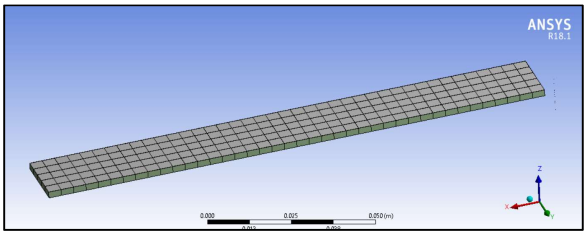

(b) Discretised FE model with boundary condition
(all displacement components $u_x = u_y = u_z = 0$ at left end)

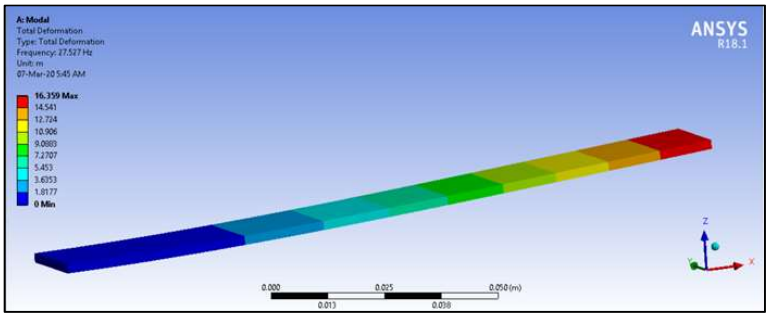

(c) First mode shape (at 27.5 Hz)

Figure 4.11. FEA model set up and first mode shape of unimorph cantilever energy harvester

Subsequently, in the second stage, numerical simulations were carried out on CEH subjected to a harmonic base structural excitation at the fixed end with an acceleration level of 9.8 m/s^2 i.e. at 1g with a frequency varying from 10 Hz to 50 Hz under a load resistance of 102 kΩ. The plots for the voltage, current and power generated with respect to the excitation frequency are shown in Figure 4.12. It is observed that the energy harvested is maximum when the base excitation matches the CEH's natural frequency. The corresponding maximum voltage, current and power harvested are 0.32 V, 3.15 μA and 1.04 μW, respectively. It can be noted here that although the modal analysis of CEH resulted in 27.5 Hz (as seen in Figure 4.11c) as the fundamental natural frequency which was also used for exciting the base structure harmonically, the maximum response of voltage, current and power occurred at 26.5 Hz, i.e. 1 Hz before the computed natural frequency. The reduction of 1 Hz in present simulation is due to the inclusion of load resistors which was not considered in the first stage of analysis i.e. modal analysis. As the harvested energy is maximum only at resonant frequencies, it can be concluded based on predicted response that the fundamental frequency of CEH including load resistors is 26.5 Hz only.

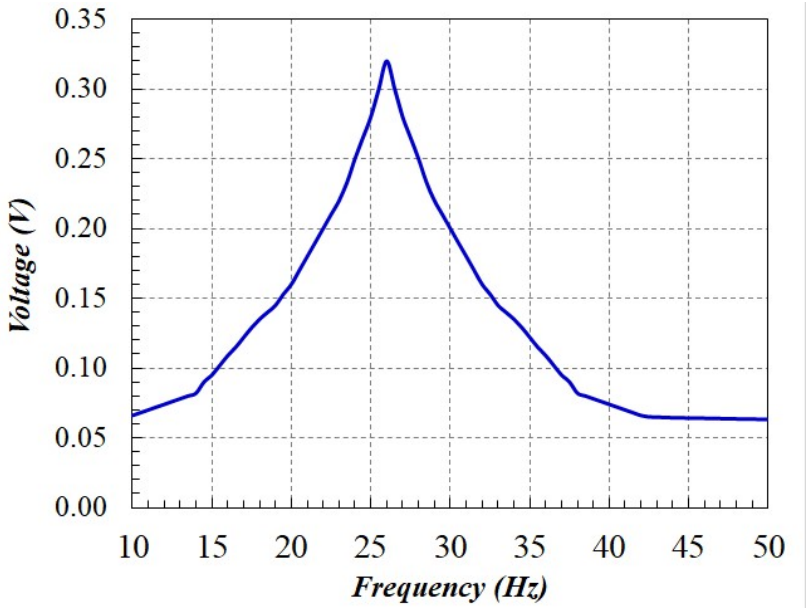

(a) Voltage output

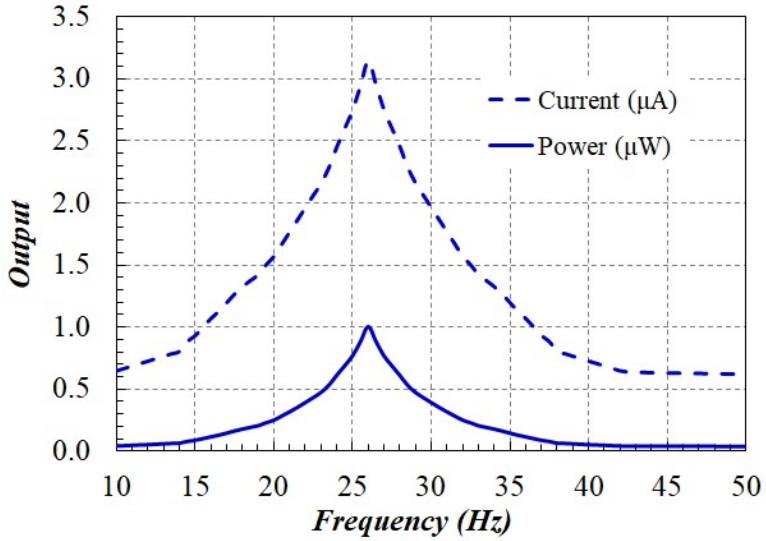

(b) Current (μA) and power output (μW)

Figure 4.12. Energy harvested from CEH for R=102 kΩ under harmonic excitation

In the third stage, the simulations were repeated twice with two more additional resistances of 150 kΩ and 260 kΩ with frequency of excitation varying from 10 Hz to 50 Hz and at 1g acceleration level to understand the performance with increase in load resistances. The predictions reveal that the harvested energy is always maximum when CEH is excited at its natural frequency, irrespective of the magnitude of the load resistance. As the load resistance is increased, the voltage output increases and the current generated decreases. Maximum voltages

of 0.32 V, 0.37 V and 0.49 V and maximum currents of 3.15 µA, 2.45 µA, and 1.85 µA were generated, respectively at load resistances of 102 kΩ, 150 kΩ and 260 kΩ as shown in Figures 4.13(a-b). On the other hand, as the load resistance is increased, the power generated decreases but the decrease is only marginal or negligible at 150 kΩ and 260 kΩ. The power generated is 1.04 µW at 102 kΩ and it is only 0.93 µW at 150 kΩ and 260 kΩ as shown in Figure 4.13(c). This demonstrates that the power generated is almost constant beyond 150 kΩ of load resistance when base is excited with 1g acceleration.

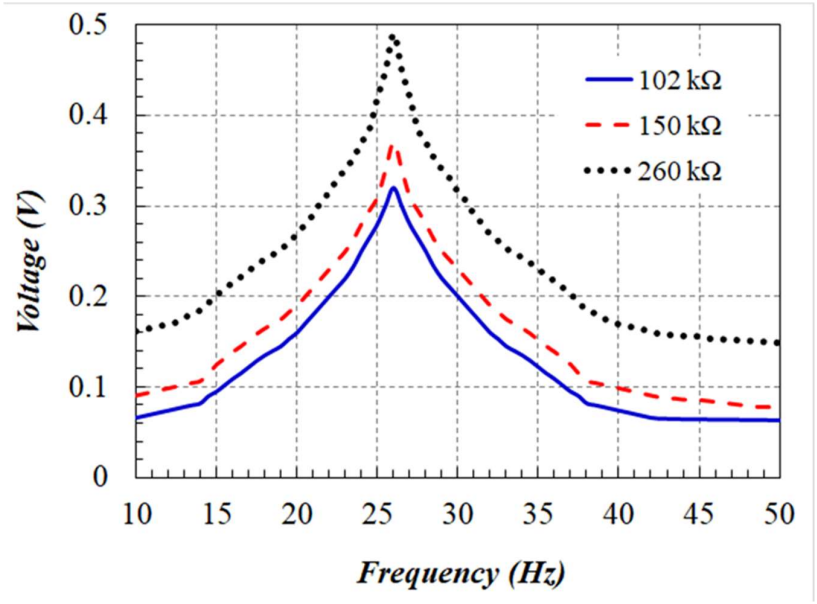

(a) Voltage output

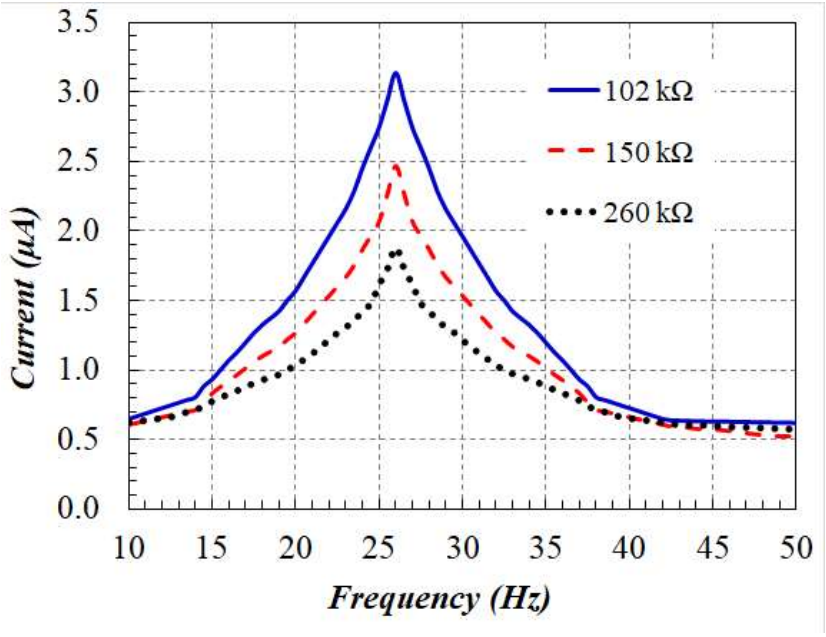

(b) Current output

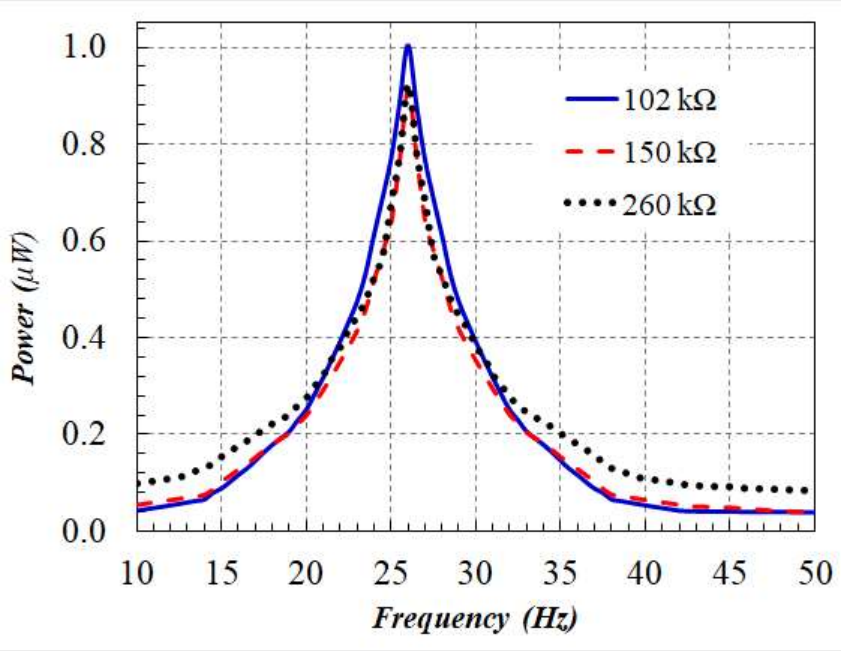

(c) Power output

Figure 4.13. Predicted frequency response of harvested energy for different load resistances under harmonic excitation

4.3.4. Numerical simulation under 1g-10g with different load resistances

Further, simulations were carried out by exciting the base structure of CEH harmonically at natural frequency and at different acceleration levels varying from 1g to 10g with load resistance as 102 kΩ. This is repeated with two more additional load resistances of 150 kΩ and 260 kΩ to investigate the harvested energy at increasing acceleration levels and increasing load resistances. All excitations were carried out at natural frequency in order to quantify the maximum possible energy output. Figures 4.14(a-c) respectively show the plots of maximum voltage, current and power generated by the CEH at three different load resistances with respect to increasing base acceleration. As the load resistance is increased, the voltage output increases and the current and power generated decreases at any given acceleration level but the voltage, current and power generated increases with the increase in base acceleration. It is to be noted that the decrease in power output when load resistances are increased is predominantly visible only at higher acceleration levels as seen in Figure 4.14(c). On contrary, this decrease with increase in load resistance beyond 150 kΩ is negligible at 1g level of base acceleration as seen in Figure 4.13(c).

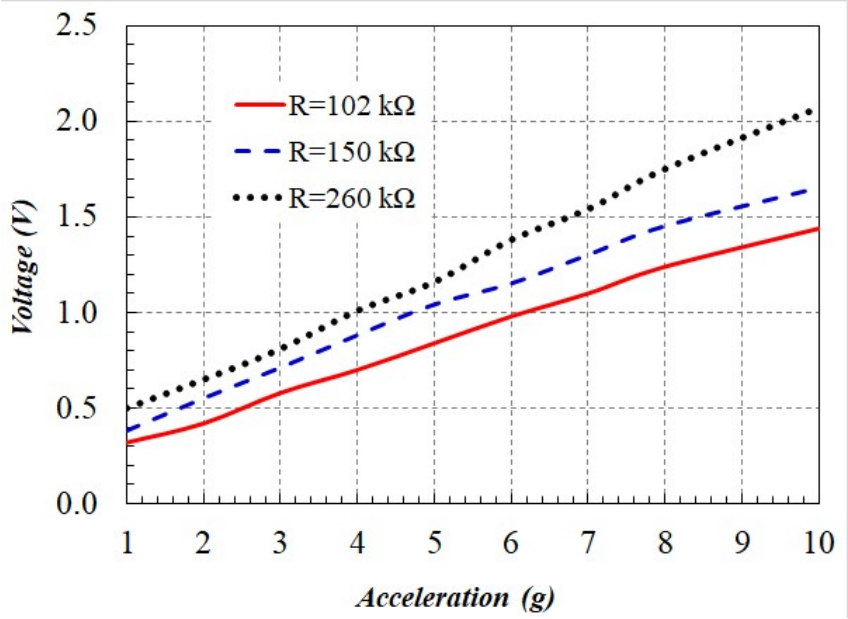

(a) Voltage output

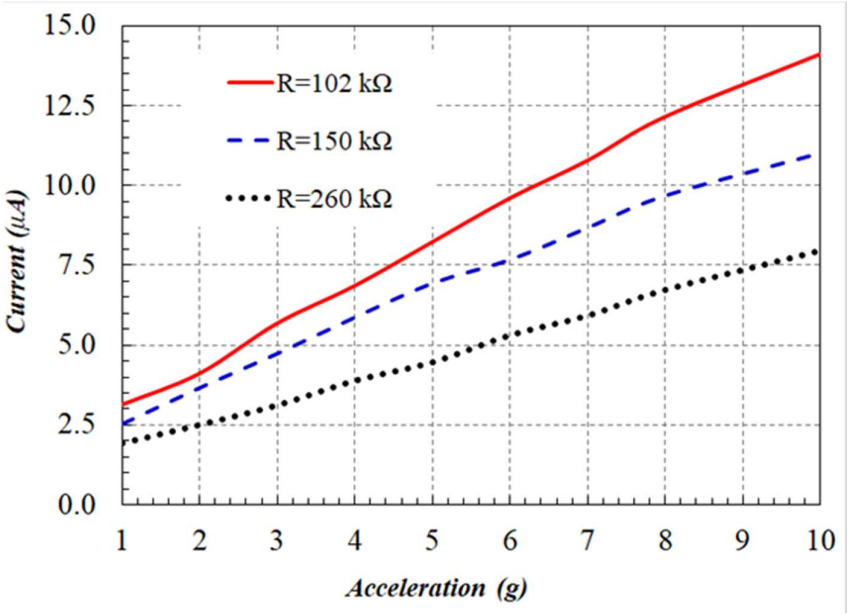

(b) Current output

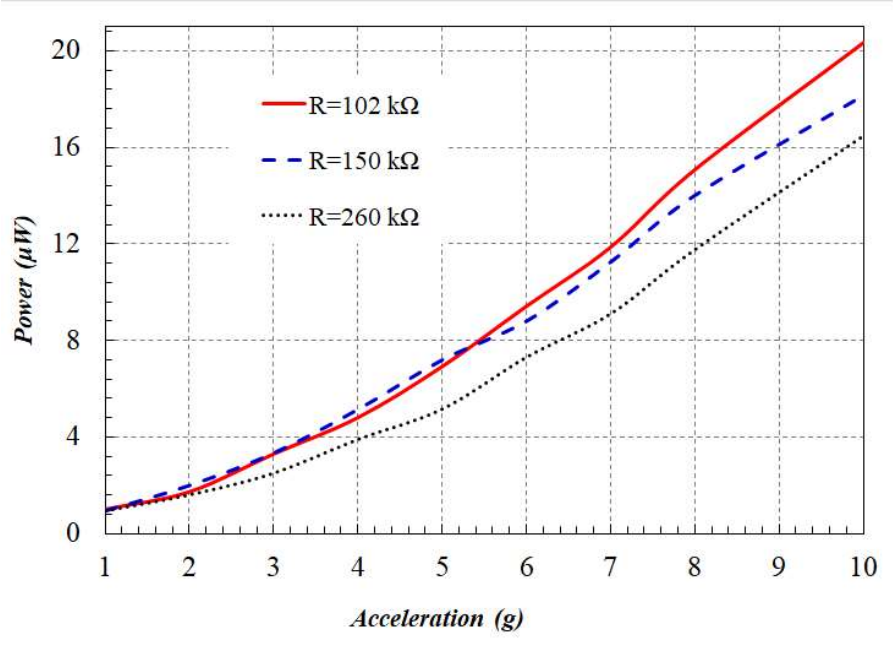

(b) Power (μW)

Figure 4.14. Predicted acceleration response of energy harvester for different load resistances under harmonic excitation

The increase in voltage output is from 0.32 V to 1.44 V with increase in base acceleration from 1g to 10g at 102 kΩ of load resistance. The corresponding increase is from 0.38 V to 1.65 V and 0.5 V to 2.07 V, respectively at load resistances of 150 kΩ and 260 kΩ as shown in Figure 4.14(a). The increase in current output is from 3.1 μA to 14.1 μA, 2.5 μA to 11.0 μA and 1.9 μA to 7.9 μA, respectively at load resistances of 102 kΩ, 150 kΩ and 260 kΩ as shown in Figure 4.14(b). The increase in power output is from 1.0 μW to 20.3 μW, 0.96 μW to 18.15 μW and 0.96 μW to 16.5 μW, respectively at load resistance of 102 kΩ, 150 kΩ and 260 kΩ with increase in base acceleration from 1g to 10g as shown in Figure 4.14(c).

4.4. Summary

The following conclusions can be drawn from the studies discussed in this chapter.

- The harvested energy is maximum when the harvester is in resonance with base excitation.
- The harvested energy increases with increase in magnitude of base accelerations.
- The voltage across the circuit, current and power generated by energy harvester increases with increase in base acceleration.

- Under increasing load resistance at any given base acceleration, the harvested voltage increases and the current and power decrease.
- The decrease in power harvested with increase in load resistance under harmonic excitation is predominantly distinguishable with increasing base acceleration.
- When the proof mass is increased from 0 to 1000 mg, the natural frequency monotonically follows a decreasing trend irrespective of beam width. The natural frequency with a given proof mass is lower for lower beam width and higher for higher beam width whereas the power output increases with decrease in beam width when the proof mass is increased from 200 mg to 1000 mg.
- The stresses that are predominant when the harvester is exposed to acceleration are bending stresses in PZT-5A and structural steel, and shear stress in mid - adhesive plane. These stresses increase linearly with respect to proof mass and reduction in beam width (Figure 4.7). These are well within the permissible limits at 1g base acceleration.
- The feasible options analyzed for maximum performance of the harvester reveals that the harvester generates a maximum power output of 880 mW and a maximum voltage of 140 V at a load of 12 kΩ when the beam width = 10 mm, proof mass = 500 mg, and resonant frequency of structure = 77.5 Hz, when exposed to the base acceleration of 30 g.

5

Experimental Validation of FEA Simulations under Harmonic Excitations

5.1. Introduction

The studies on CEH performed and mentioned in the previous chapter gave sufficient understanding on performance of harvesting structure under harmonic excitation and procedure for carrying out the finite element analysis as well. During those studies, the reference for geometry and material is taken from literature in which the harvesting structure and piezoelectric material are not physically available in the market. In order to carry out experimental investigations for validation of numerical results, the numerical simulation of such a geometry and material is executed which is readily available in market. The same CEH is experimented by subjecting its base to a harmonic excitation with increasing levels of accelerations, individually at three different load resistances of 102 kΩ, 150 kΩ and 260 kΩ.

5.2. Experimental setup

The experimental setup is established as per the block diagram shown in Figure 5.1(a). Actual experimental setup is shown in Figure 5.1(b) and the details of CEH mounted over the vibration Shaker is shown in Figure 5.1(c). An accelerometer is mounted over the Shaker for

controlling the input excitations in closed loop. The equipment employed in experimental set up is briefly described here.

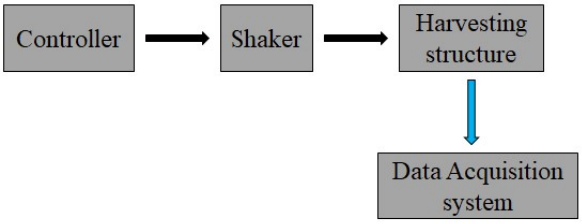

(a) Block diagram of experimental setup

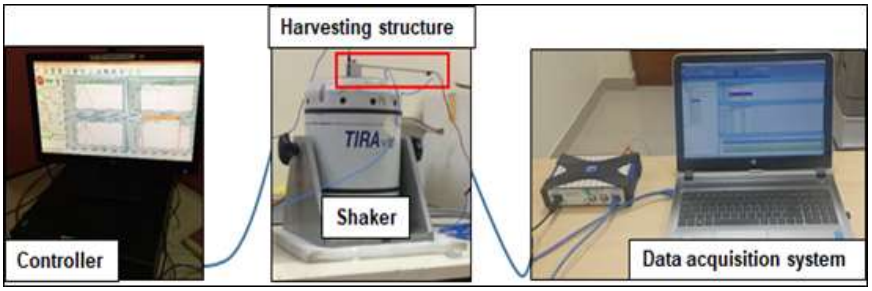

(b) Actual experimental setup

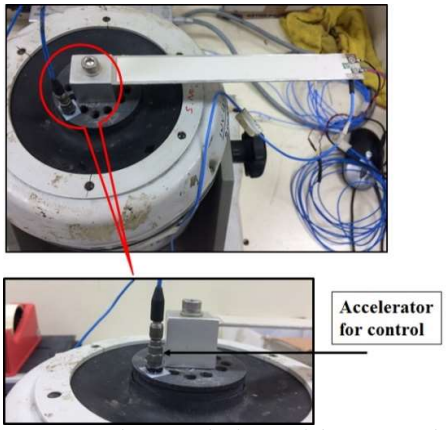

(c) Energy harvester mounted over shaker with an accelerometer for control

Figure 5.1. Experimental set-up

Shaker with controller: The vibration shaker with inbuilt controller is used for imparting the specified vibration. The shaker is electrodynamic type in which the vibrations are generated from electricity influencing the magnetic flux generated in armature. The details of vibration shaker are make: Sdyn, model: SEV 360, and capacity: 3.5 tonnes.

Energy harvester: It consists of a piezoelectric unimorph. The piezoelectric material used in present study is a semi-crystalline PVDF (Polyvinylidene fluoride), LTD4-28K/L of 40 μm

thickness and bonded over an aluminium alloy AA2014 base cantilever beam of dimensions 171x22x2 mm as shown in Figure 4.10(a) in which the geometry of the harvesting structure with piezoelectric layer is shown in red color and aluminum substructure in grey color. A ϕ6 mm hole is provided at the fixed end of this harvester for clamping with the base exciting structure. The piezoelectric material is bonded to the aluminium substructure by cyanoacrylate adhesive Mbond 200. The actual configuration of the harvester is shown in Figure 4.10(b). The properties of PVDF taken from manufacturer's data sheet are given in Table 4.3. The properties of aluminum alloy used for substructure is mentioned in Table 4.4. The energy harvester is a cantilever type. The piezoelectric material is PVDF of 40 μm thickness bonded over an AA 2014 beam of 171mm x 22mm x 2mm dimensions.

***Data acquisition system (DAS)*:** The DAS is employed to measure the voltage across the circuit and record the same when the CEH is subjected to specified vibrations. The details of DAS are make: HBM make, model: MX1601B.

5.3. Experiments

The experiments were carried out in two stages under harmonic excitations to validate the corresponding numerical simulations discussed in Section 4.3 in Chapter-4. In the first stage, CEH was subjected to a harmonic base structural excitation at the fixed end with an acceleration level of 1g at a frequency varying from 10 Hz to 50 Hz with a load resistance of 102 kΩ. The fundamental natural frequency of 26.5 Hz was obtained for the CEH from the measured frequency response. In the second stage, experiments were carried out by exciting the base of CEH harmonically at natural frequency with different acceleration levels varying from 1g to 10g with load resistance as 102 kΩ. This was repeated with two more additional load resistances of 150 kΩ and 260 kΩ to experimentally investigate the harvested energy at increasing acceleration levels and increasing load resistances.

5.3.1. Harmonic excitation at 1g with a load resistances

The CEH was mounted over the vibration table on top of the Shaker. The vibration table acts as a base structure for the CEH. An accelerometer was additionally mounted on top of the vibration table away from CEH as shown in Figure 5.1(c). This was mounted to feedback and control the achieved vibration level in a closed loop control system. The terminals of PVDF on unimorph CEH were connected to the two equal load resistors of $R_a = R_b = 51$ kΩ and (R=Ra + R_b) and then to the DAS as shown in Figure 5.2, which in turn was connected to the Computer.

At 1g level of acceleration, the Shaker was programmed and provided a harmonic excitation to the vibration table starting from 10 Hz until 50 Hz. This range was finalized based on predicted fundamental natural frequency from numerical simulations, discussed in Sec-4.3.3 in Chapter-4. This frequency range covered the base excitation of approximately ±20 Hz with respect to the natural frequency of 27.5 Hz of the CEH.

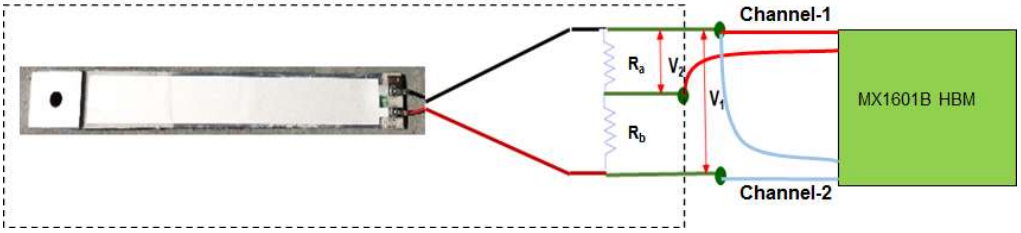

Figure 5.2. Experimental measurement setup for harvested voltage

The voltage generated in CEH across the two channels V_1 and V_2 were recorded. From the recorded voltages, the current 'i', was calculated through Ohm's law as $i = \frac{V_2}{R_a}$. The power P was calculated as $P = i^2 R$. The voltage across the circuit, current and power generated from CEH are plot in Figures 5.3(a-b).

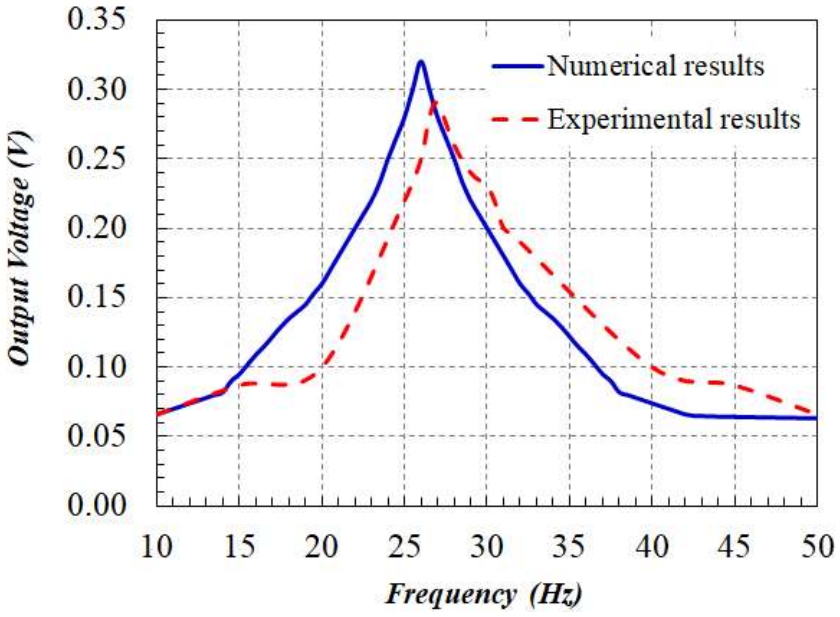

(a) Voltage output

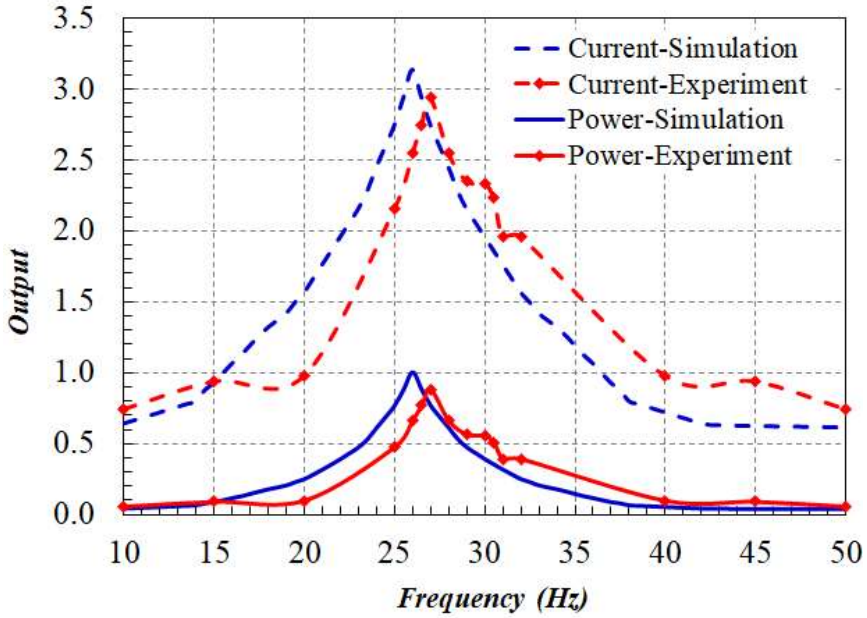

(b) Current (μA) and power output (μW)

Figure 5.3. Energy harvested from simulation versus experiment for R=102 kΩ under harmonic excitation

5.3.2. Harmonic excitations from 1g-10g with three different load resistances

The results of aforementioned simulations (Chapter-4) and experiments have shown that the harvested energy is maximum when the harvesting structure is in resonance with base excitation. Therefore, the experiments were carried out by exciting the base structure of CEH harmonically at 27.5 Hz i.e. at natural frequency with different acceleration levels varying from 1g to 10g with load resistance R = 102 kΩ. The voltages generated across two channels V_1 and V_2 were measured and recorded. Similar to the procedure mentioned in Sec-5.3.1, the current and power generated from each acceleration level of excitation were computed. This experiment was repeated with two more additional load resistances of 150 kΩ and 260 kΩ individually to experimentally investigate the harvested energy at increasing acceleration levels and increasing load resistances. The voltage, current and power harvested from CEH under increasing acceleration levels from 1g to 10g for three load resistances 102 kΩ (R_a= R_b = 51 kΩ), 150 kΩ (R_a= R_b = 75 kΩ) and 260 kΩ (R_a= R_b =130 kΩ) are showed in Figures 5.4(a-c).

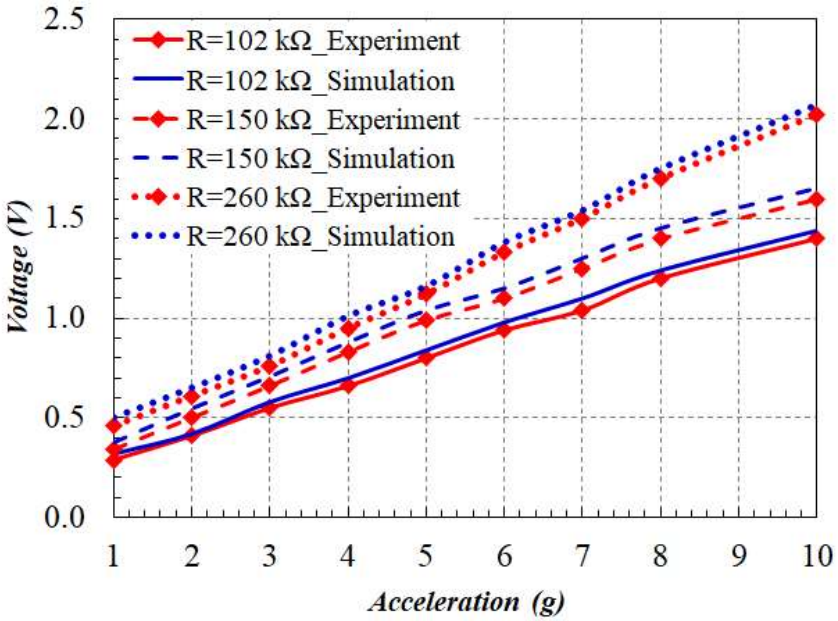

(a) Voltage output

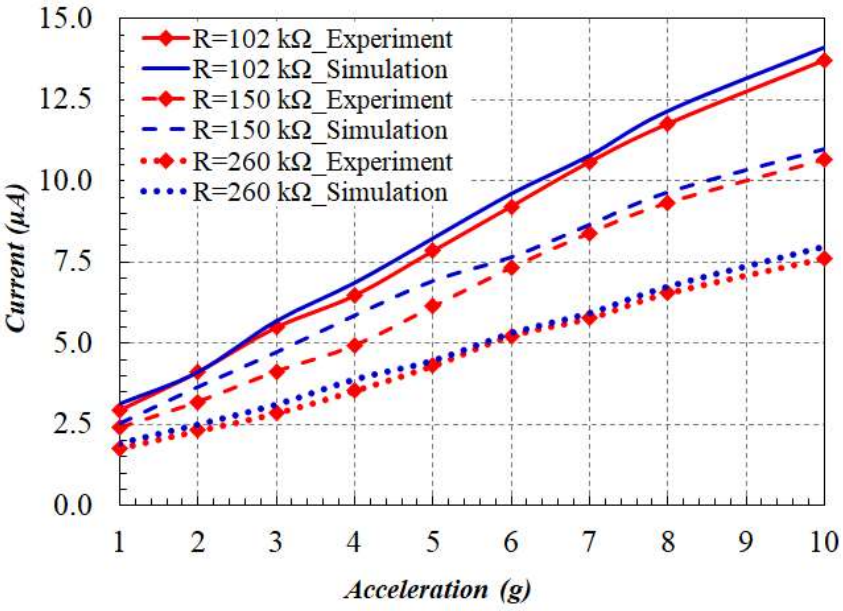

(b) Current output

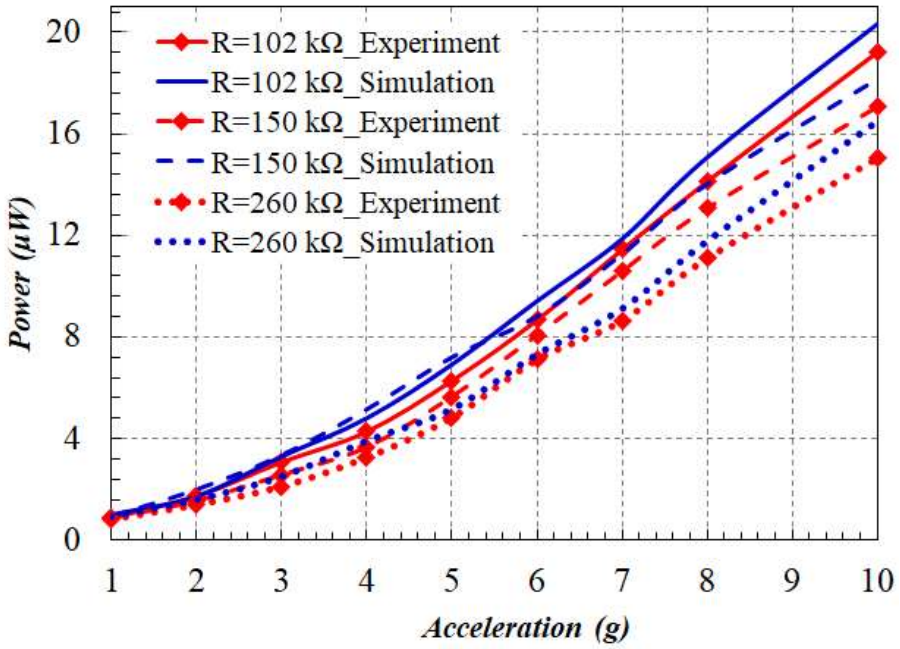

(c) Power (μW)

Figure 5.4. Effect of base acceleration on harvested energy under harmonic excitation for three different load resistances

5.4. Comparison of experiments and simulations

The results from numerical simulations and experiments on CEH under base structural harmonic excitation are compared here. Initially, the frequency response of CEH under harmonic excitation ranging from 10 Hz to 50 Hz at an acceleration level of 1g for a load resistance of 102 kΩ are compared in Figures 5.3(a-b). Although the experimental results were closely matching with results of numerical simulations, the numerical simulations slightly over predicted the maximum responses occurred at resonance for the load resistance. Even the fundamental natural frequency of CEH including load resistors predicted from simulation is 26.5 Hz against the experimentally determined value of 27.5 Hz. This difference of 1.0 Hz in experimental value of natural frequency may be attributed to slight difference in mass of CEH due to wire terminals connecting the CEH to the DAS and mass of resistors in the circuit. Due to the same reason, there is a slight reduction in maximum harvested energy at resonance in experiments. However, it can be observed that the area under the curve of power generated from experiment and simulation shown in Figure 5.3(b) remains almost same which represents that the energy harvested is same irrespective of the above said differences between experiment and simulation in terms of maximum harvested energy and natural frequency.

Secondly, the acceleration response of CEH in terms of voltage, current and power under harmonic excitation varying from 1g to 10g for different load resistances 102 kΩ, 150 kΩ and 260 kΩ is compared in Figures 5.4(a-c). The experimental results have very good agreement with numerical simulation results. The plots show that as the load resistance increases, the voltage across the circuit increases whereas the current and generated power decreases. However, the reduction in power generated is insignificant beyond 150 kΩ load resistance as shown in Figure 5.4(c). All results clearly show that the harvested energy increases with increase in base acceleration levels. However, the trend in increase in voltage and reduction in generated current and power with the increase in load resistances are same as observed in 1g acceleration level. The decrease in power output with increase in load resistance is predominantly visible with increase in base acceleration levels as seen in Figure 5.4(c).

5.5. Summary

The experimental investigations were carried out to validate the results of numerical simulation. The experiment employed the vibration Shaker of capacity 3.5 tons, energy harvester and data acquisition system. The experiments were carried out by subjecting the CEH connected to different loads to harmonic excitation. Initially, the investigations were carried out for frequency response of CEH connected to 102 kΩ and subjected to 1g excitation for the frequencies ranging from 10-50 Hz in which the experimental results closely matched the results of numerical simulations. The natural frequency of CEH along with load resistors predicted from simulation was 26.5 Hz against the experimentally determined value of 27.5 Hz. This difference of 1.0 Hz in experimental value of natural frequency may be attributed to slight difference in mass of CEH due to wire terminals connecting the CEH to the DAS and mass of resistors in the circuit. Due to the same reason, there is a slight reduction in maximum harvested energy at resonance in experiments. However, it can be observed that the total power generated from experiment and simulation remains almost same.

Further, investigation on acceleration response of CEH was carried out where it was subjected to different harmonic excitations ranging from 1g to 10g at its natural frequency 27.5 Hz. The experimental results of CEH connected to different load resistances exhibited very good agreement with that of numerical results. It is inferred from the investigation that, with the increase in load resistance, the voltage across the circuit increases whereas the current and generated power decreases. The decrease in power output with increase in load resistance is

predominantly visible with increase in base accelerations, and with increase in base accelerations, the voltage, current and power increases.

6

Performance evaluation of CEH under harmonic and random excitations

6.1. Introduction

Sufficient understanding on energy harvesters subjected to harmonic excitation is obtained from the work done in the previous chapters. The relative performance of the cantilever energy harvester under harmonic and random excitations is not yet well understood in literature and a very limited work is carried out on energy harvesters under random excitations. This chapter focuses on the behavior of energy harvester under the influence of random vibration, characterization of the energy harvester for maximum power output and evaluation the performance of same energy harvester under the influence of harmonic and random vibrations.

6.2. Experimental setup

The experimental setup is established as per the block diagram shown in Figure 5.1(a). It is same as the one used for studies of energy harvester under harmonic excitation. The actual experimental setup is shown in Figure 5.1(b) and the details of CEH mounted over the vibration Shaker is shown in Figure 5.1(c). An accelerometer is mounted over the Shaker for controlling the input excitations in closed loop. The equipment employed in experimental set up is same as the ones described in Sec-5.2.

6.3. Experiment on CEH under random excitations

The CEH was experimented by subjecting its base to a random excitation with frequency bandwidth ranging from 10 Hz to 100 Hz with acceleration spectral density ranging from 0.011 g^2/H_z to 0.71 g^2/H_z. The range of adopted acceleration spectral density corresponds to an increasing level of equivalent accelerations (root mean square, i.e. RMS) ranging from $1g_{rms}$ to $8g_{rms}$. The frequency bandwidth is selected to cover up to at least three times the measured fundamental natural frequency of 26.5 Hz. The experimental setup, the method of measurement, recording of voltages and computation of generated current and power from recorded voltages are same as adopted in previous experiments under harmonic excitation explained in Chapter 5. The experiments were conducted individually at each acceleration level ($1g_{RMS}$ to $8g_{RMS}$) at a load resistance of 102 kΩ. This experiment was repeated with two more additional resistances of 150 kΩ and 260 kΩ.

The results generated from random excitation are shown in Figures 6.1(a-c). The voltage across the circuit, current and power generated increases with the increase in the base excitation i.e. base acceleration level for any given load resistance. When the load resistance increases, the voltage and power generated increase and the current generated decreases.

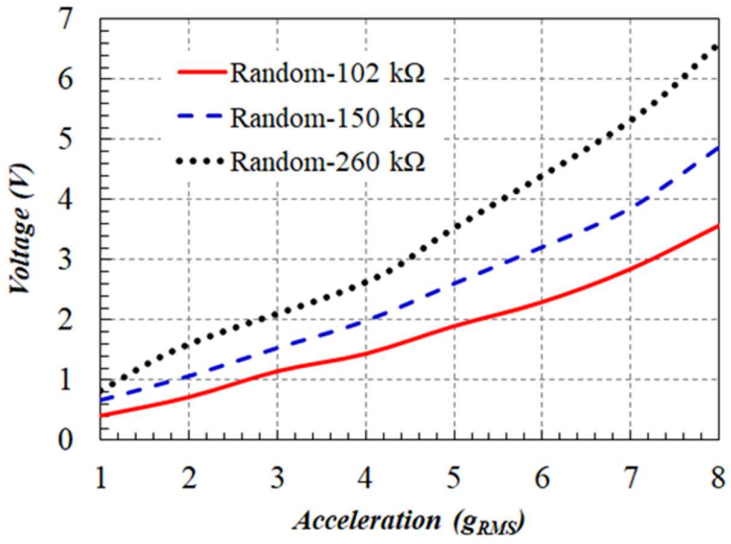

(a) Voltage output g_{RMS}

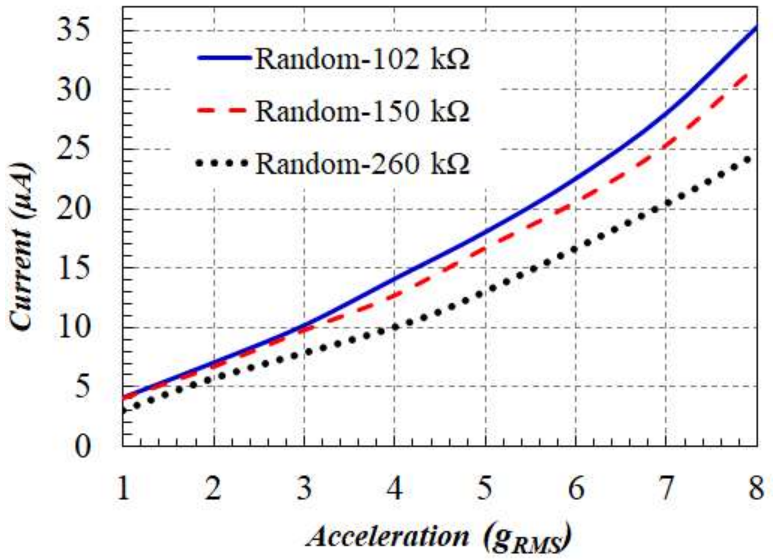

(b) Current output

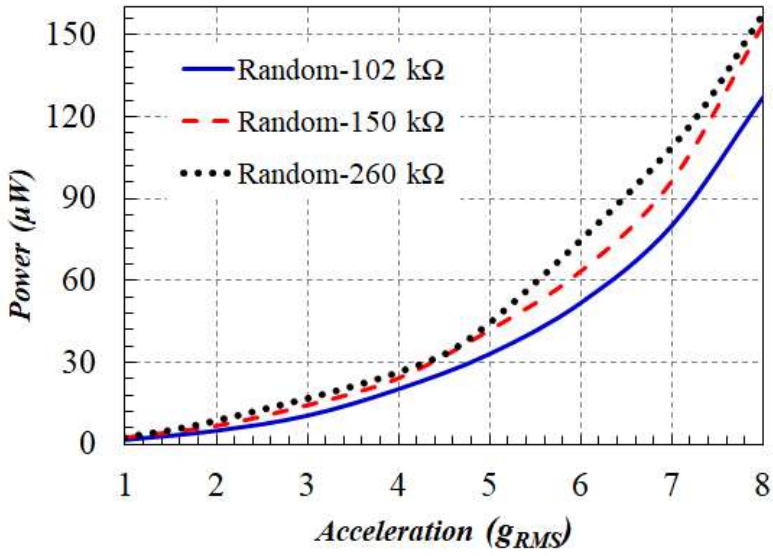

(c) Power output

Figure 6.1. Effect of base acceleration on harvested energy under random excitation for three different load resistances

6.4. Comparison of harvested energy under random and harmonic vibrations

The experimentally harvested energy from CEH under harmonic and random vibrations (i.e. base excitations) with increase in base acceleration levels for three different load resistances are shown in Figures 6.2(a-c). The range of harvested energy (voltage, current and

power) with the increase in acceleration levels under both excitations for three load resistances are shown in Table 6.1. These comparisons clearly demonstrate that the equivalent random excitation yields higher energy output and the harvested energy increases almost parabolically with increase in base accelerations as compared to linear increase in harvested energy in the case of harmonic excitation.

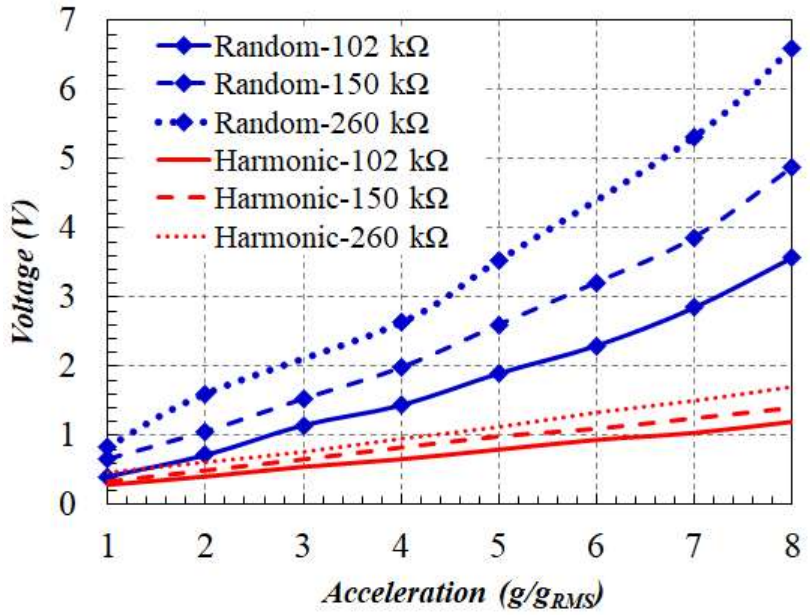

(a) Voltage output

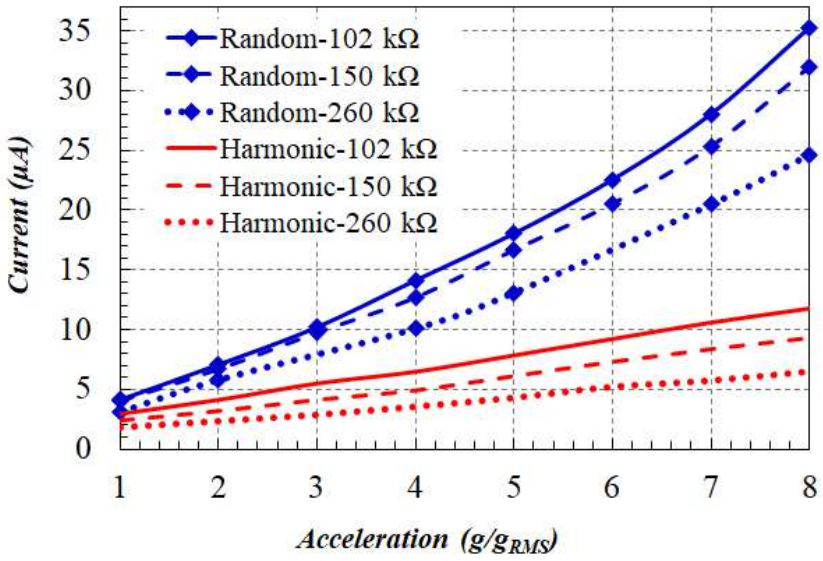

(b) Current output

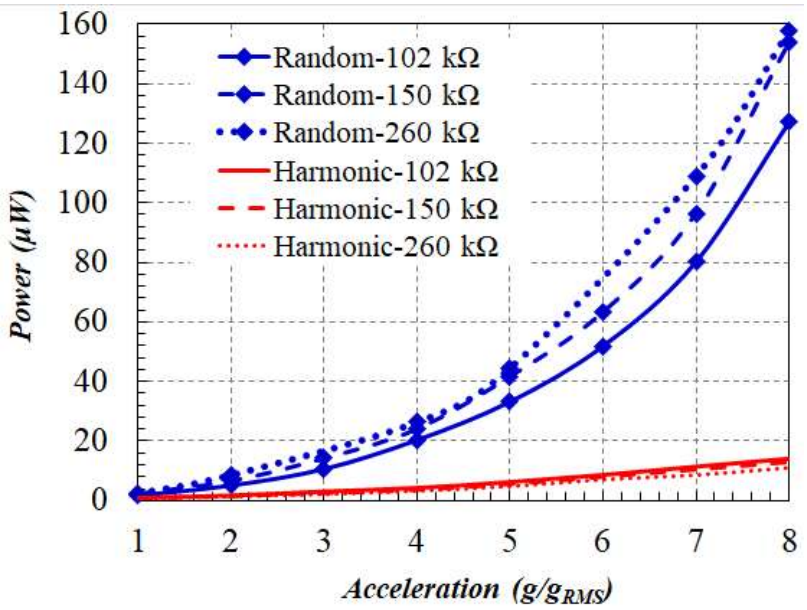

(c) Power output

Figure 6.2. Harvested energy under random versus harmonic excitations for three different load resistances, under increasing base acceleration

Table 6. 1. Range of harvested energy under harmonic and random excitations under increasing acceleration levels from 1g to 10g from experiments

S.No.	Load (kΩ)	Harmonic excitation			Random excitation		
		Voltage (V)	Current (μA)	Power (μW)	Voltage (V)	Current (μA)	Power (μW)
1	102	0.30 – 1.20	2.90 – 11.70	0.88 – 14.11	0.40 – 3.60	4.1 – 35.0	1.70 – 127.0
2	150	0.34 – 1.40	2.40 – 9.30	0.86 – 13.06	0.60 – 4.80	4.0 – 32.0	2.40 – 154.0
3	260	0.46 – 1.70	1.70 – 6.50	0.81 – 11.11	0.80 – 6.60	3.0 – 24.0	2.46 – 157.0

6.5. Summary

The work in this chapter investigated the cantilever energy harvester made of PVDF and aluminum in unimorph configuration. The relative performance of harvester in terms of amount of energy harvested when subjected to random vibration and equivalent harmonic motion is clarified here which was not well understood in literature. The performance of this energy harvester was experimentally studied under random excitations. The following important conclusions can be drawn from this chapter.

- The harvested energy increases with increase in magnitude of base excitation irrespective of the type of excitation.

- Under increasing load resistance at any given base acceleration, the harvested voltage increases and the current and power decrease in the case of harmonic excitation, whereas the harvested voltage and power increase and the current decreases in the case of random excitation.
- The power harvested is 2-14 times higher in random excitations when compared with that of equivalent harmonic excitations, with increase in equivalent base accelerations ranging from 1g to 8g for three different loads adopted in experiments.
- This cantilever energy harvester is recommended to be used in aerospace industry especially in structures where random vibration is predominant.

7

Implementation of CEH in an airframe section subjected to broadband random vibrations

7.1. Introduction

Considerable amount of research has been carried out on cantilever energy harvester in stand-alone mode in the past when subjected to harmonic and random excitations [15, 16, 19, 36, 37, 38, 39, 40, 28]. Few researchers [38, 39] have developed computational models to study the performance of CEH subjected to random excitation. But the performance of this CEH is unknown when this harvester is subjected to different bandwidth of random excitations at the base. In this chapter, experiments have been carried out to investigate the influence of frequency bandwidth of the random base excitation on the output of the CEH when the harvester is mounted inside an airframe section. The schematic diagram of CEH mounted in an airframe is shown in Figure 7.1. Further, the harvesters' performance is studied at different loads at each frequency bandwidth and under different acceleration levels.

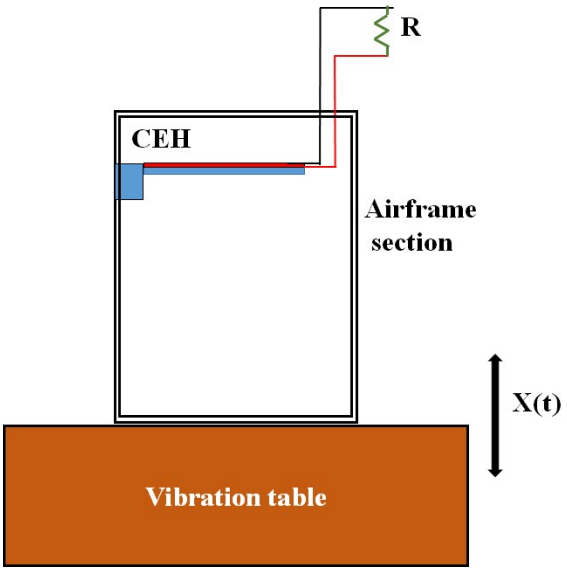

Note: R = load resistance; X(t)= base excitation

Figure 7.1. Schematic diagram of an airframe section with CEH under base excitation

7.2. Properties of CEH and airframe section

The configuration of CEH in the present study is similar to that of the one studied in previous chapters. The energy harvester consists of a cantilever beam structure with piezoelectric patch glued to the upper surface. The piezoelectric patch used is a PVDF having Part No. LTD4-28K/L. The patch has a thickness of 40 μm. It is glued to the aluminum alloy material (AA2014) cantilever beam whose dimensions are shown in Figure 5.2(a). In the figure, the piezoelectric material is indicated by red colour and the aluminium alloy beam is indicated by grey colour. The base kind of structure is provided to the beam so that the beam can be clamped to the vibration table and airframe section using M6 fastener. Mbond 200 is used for gluing PVDF to aluminium alloy beam. The hardware of the CEH is shown in Figure 5.2(b). The Table-5.1 and 5.2 in Chapter-5 gives the details of the properties of piezoelectric material that is provided by manufacturer and the aluminium alloy material.

Further, the CEH is mounted in airframe section. The airframe section is made up of aluminium alloy AA2014. The dimensions of airframe section and configuration for experiment are detailed in Figure 7.2(a) and 7.2(b) respectively. The properties of AA2014 is shown in Table 6.1. The CEH is mounted in airframe section using M6 fasteners at its front bulkhead.

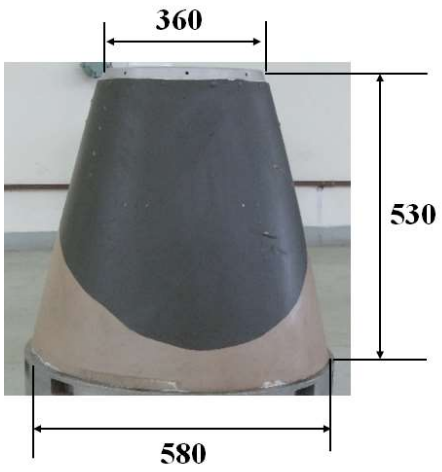

(a) Dimensions of airframe section

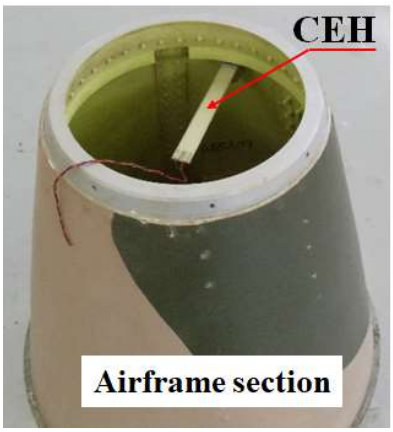

(b) CEH mounted on FBH of airframe

Figure 7.2. Airframe section with CEH

Table 7. 1. Properties of aluminum alloy (AA2014)

S. No.	Property	Value	Unit
1	Density	2650	kg/m^3
2	Young's modulus of elasticity (E)	70	GPa
3	Poisson's ratio	0.3	-

7.3. Experiment on CEH under harmonic and random excitations

The experiments are performed in three stages viz. (i) study of CEH in stand-alone mode under harmonic excitations, (ii) study of CEH mounted in an airframe section and subjected to harmonic excitation, and (iii) study of CEH mounted in an airframe section and subjected to random excitation. In stage-1, the energy harvester in stand-alone mode is subjected to a harmonic excitation of 1g at the fixed end. The frequency is swept from 10 Hz to 40 Hz without any load. The first natural frequency of the energy harvester is determined from its frequency response. In stage-2, the experiments are performed by mounting CEH in airframe section and excited the airframe structure at its base, at natural frequency of the energy harvester. Here, the airframe section is subjected to simple harmonic motion ranging from 1g to 5g with 0 Ω, 100 kΩ, 1000 kΩ and 10000 kΩ loads. In stage-3, keeping the setup same as in stage-2, the excitation is changed to random from harmonic. The frequency bandwidths for this excitation

are chosen so that the fundamental frequency of CEH lie within the selected range. The experiment is conducted at vibration levels from 1 g_{RMS} to 5 g_{RMS}.

7.3.1. Experimental setup

The block diagram as shown in Figure 7.3(a) is taken as a reference for setting up the experiment. The setup for experiments on CEH with airframe is shown in Figure 7.3(b). The Figure 7.3(c) shows the mounting details of CEH in airframe.

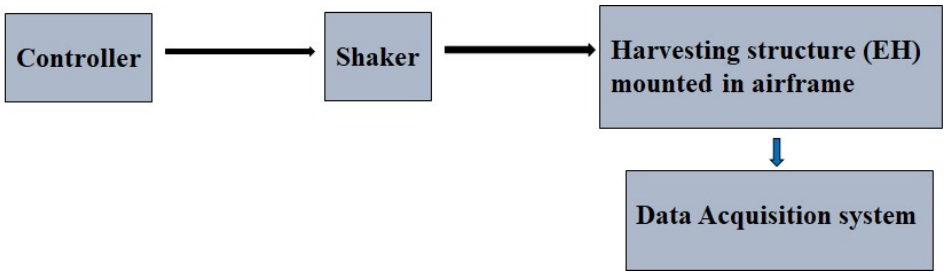

(a) Block diagram for experiment

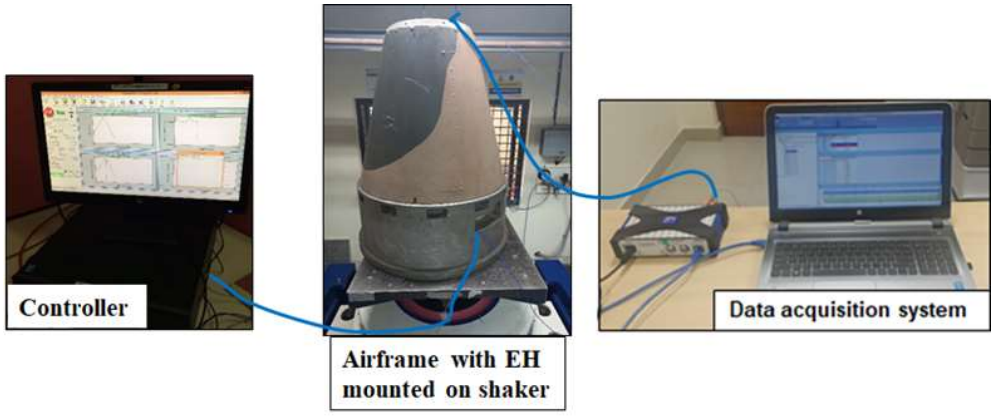

(b) Experimental set up

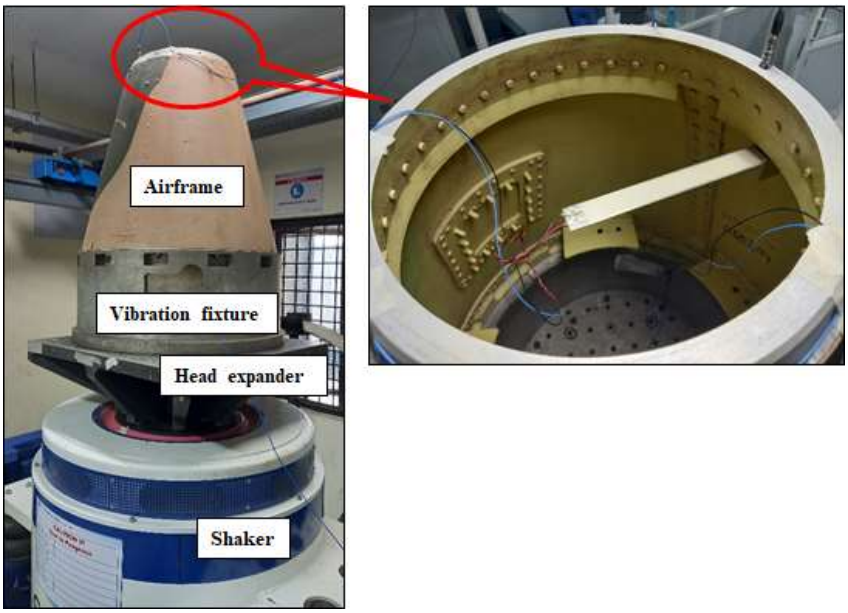

(c) CEH in airframe during experiment

Figure 7.3. Airframe on shaker

The vibration levels to the airframe during experiments is controlled by using an accelerometer. It is mounted on the vibration fixture. The various equipment used during the experiment are mentioned below.

Shaker with controller: The vibration shaker with inbuilt controller is used for imparting the specified vibration. The Shaker is an electrodynamic type in which the vibrations are generated from electricity influencing the magnetic flux generated in armature. The details of vibration shaker are make: Sdyn, model: SEV 360, and capacity: 3.5 tonnes.

***Data acquisition system (DAS)*:** The DAS is employed to measure the voltage across the circuit and record the same when the CEH is subjected to specified vibrations. The details of DAS are make: HBM make, model: MX1601B.

The two resistors with R_l value are connected in series to measure the voltages V_1 and V_2 across the circuit, as shown in Figure 7.4. The value V_2 i.e. the voltage across the single resistor is used for calculation of power and current.

Figure 7.4. Electric circuit in CEH

7.3.2. Harmonic excitation of CEH in stand-alone mode at 1g without load.

The energy harvester is mounted on the Shaker. The Shaker simulates the source of base excitation for the energy harvester. An accelerometer is mounted on the shaker on its top near to base of CEH to measure and control the base excitation so that the specified vibration levels could be transmitted to the CEH. The details are shown in Figure 7.5.

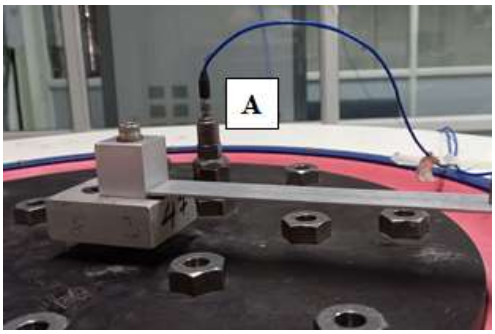

Figure 7.5. Accelerometer on Shaker

The piezoelectric material which is glued to the harvesting structure is connected to DAS as shown in experimental set up. The energy harvester is subjected to simple harmonic motion from 10 Hz to 40 Hz with a magnitude of 1g. It is inferred from the results of simulations and experiments in Chapters 4 and 5 that the energy harvester is effective when the harvesting structure is excited at its natural frequency. In the present study the harvester is effective at 34.5 Hz. The voltage across the circuit in CEH is recorded and is shown in Figure 7.6.

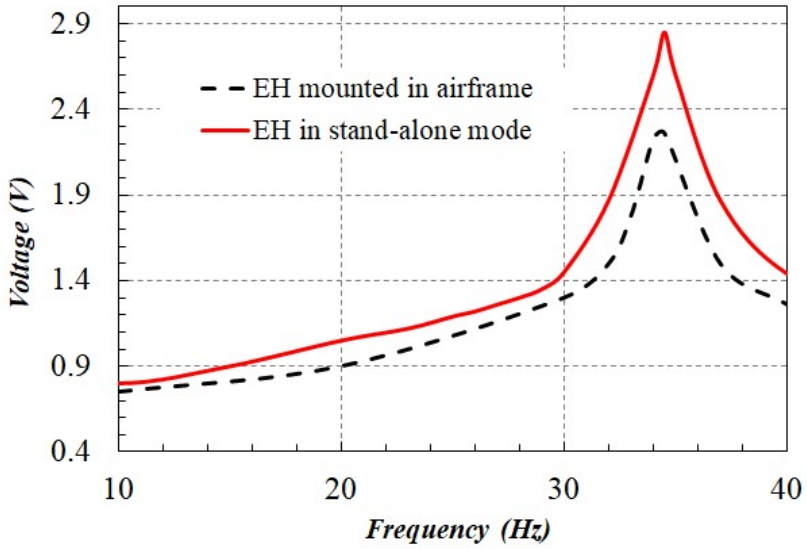

Figure 7.6. Comparison of voltage across CEH

7.3.3. Harmonic excitations of CEH mounted in airframe from 1g-5g

Further, the CEH is mounted in the airframe and the airframe in turn is mounted on the Shaker with the help of head expander as shown in Figure 7.3(c). The airframe section assembly is subjected to simple harmonic motion from 10 Hz to 40 Hz with a magnitude of 1g. The voltage generated across the channel V_1 was measured, recorded and compared with that of CEH in stand-alone mode as shown in Figure 7.6. Based on the results of the experiments performed here as well as in the previous section, the airframe was base excited harmonically from 1g to 5g at 34.5 Hz i.e. at natural frequency of CEH with 100 kΩ for generating maximum power. The voltage V_1 across the circuit is measured and recorded. The current 'i' is calculated through Ohm's law as $i=\frac{V_2}{R_l}$ and if $R= 2R_l$ then the power $P = i^2 R$. The voltage across the circuit and power generated by CEH are plotted in Figures 7.7(a-c). The procedure is repeated with two more resistances of 1000 kΩ and 10000 kΩ to investigate the harvested energy at different acceleration levels and loads. The voltage across the circuit, current and power generated from CEH at different values of excitation varying from 1g to 5g for three different loads 100 kΩ (R_l=50 kΩ), 1000 kΩ (R_l=500 kΩ) and 10000 kΩ (R_l=5000 kΩ) are shown in Figures 7.7(a-c).

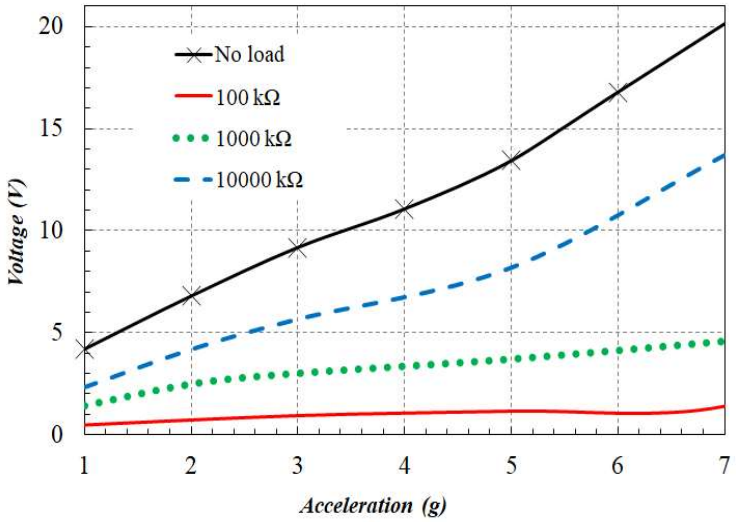

(a) Voltage across CEH

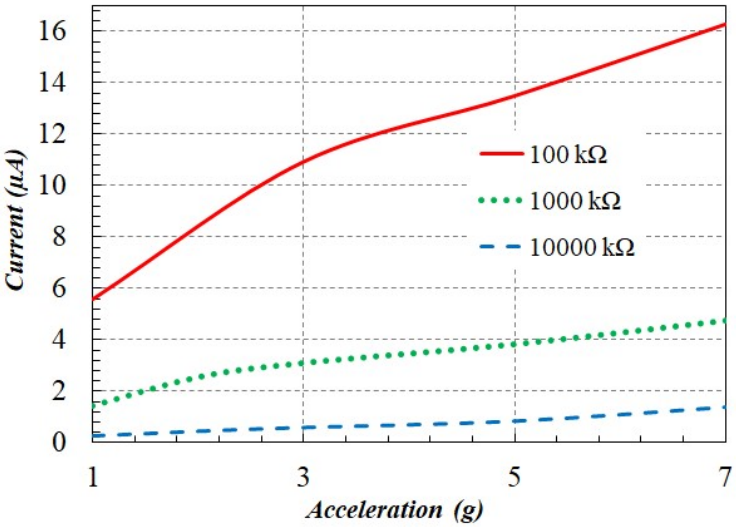

(b) Current output

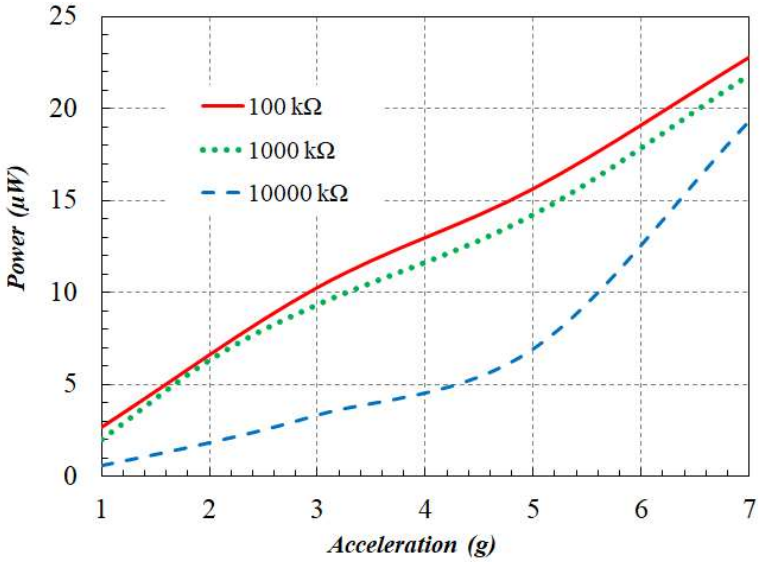

(c) Power generated

Figure 7.7. Acceleration response (Harmonic excitation) of CEH mounted in airframe

7.3.4. Random excitation of CEH mounted in airframe from 1 g_{RMS} – 5 g_{RMS}

The airframe section with CEH is further studied by conducting more experiments in which the assembly is subjected to base random excitation with four frequency bandwidths ranging from 20 - 50 Hz, 20 - 250 Hz, 20 - 500 Hz and 20 - 800 Hz with acceleration magnitudes ranging from 1 g_{RMS} to 5 g_{RMS}. The input to the vibration table is in terms of acceleration spectral density (ASD). The magnitude of ASD for the same magnitude of excitation in terms of g_{RMS} changes for different bandwidths. The calculation is shown in Eq. (7.1) and the values are mentioned in Table-7.2.

$$g_{RMS} = \sqrt{BW \times ASD} \tag{7.1}$$

$$ASD = \frac{g_{RMS}^2}{BW} \tag{7.2}$$

where ASD is expressed in g^2 / Hz, BW is the frequency bandwidth in HZ, and g_{RMS} is the acceleration in terms of g.

Table 7. 2. ASD from g_{RMS}

S. No.	Frequency bandwidth (Hz)	Magnitude of excitation (g_{RMS})	Acceleration spectral density (g^2 /Hz)
1	20-50	1	0.030
		3	0.300
		5	0.830
2	20-250	1	0.004
		3	0.039
		5	0.100
3	20-500	1	0.002
		3	0.018
		5	0.052
4	20-800	1	0.001
		3	0.010
		5	0.030

The bandwidth of frequencies is chosen to consider the frequencies of all the vehicles that move in air, water and land. Frequencies in the range of 20-50 Hz, 20-250Hz, 20-500Hz and 20-800 Hz are experienced by automobiles and ships, helicopters, aero planes and missiles respectively. The procedures mentioned in the section 7.3.3 on *"harmonic excitations of CEH mounted in airframe"* is adopted for measuring voltage, calculation of current and power from voltages with same experimental setup for the studies. Here, the airframe section assembly is subjected to different values of excitation ($1g_{RMS}$, $3g_{RMS}$ and $5g_{RMS}$) connected to a load of 100 kΩ in a frequency bandwidth 20-50 Hz. The process is repeated with another two loads of 1000 kΩ and 10000 kΩ in above mentioned frequency bandwidths. The acceleration response of CEH from random excitation are shown in Figures 7.8 (a-c) and frequency bandwidth response of CEH are shown in Figure 7.9 (a-c). The power generated increases with the increase in magnitude of vibration levels irrespective of loads. The voltage across the circuit increases, the current and power generated decreases with increase in load. This trend is observed in all the frequency bandwidths but the magnitude of power generated is relatively high in low frequency bandwidth with low magnitude that is 20-50Hz.

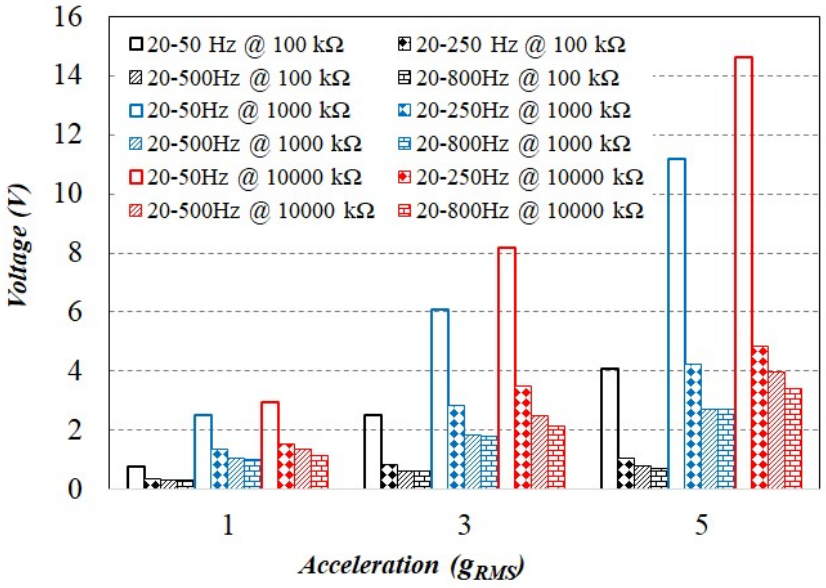

(a) Voltage across CEH

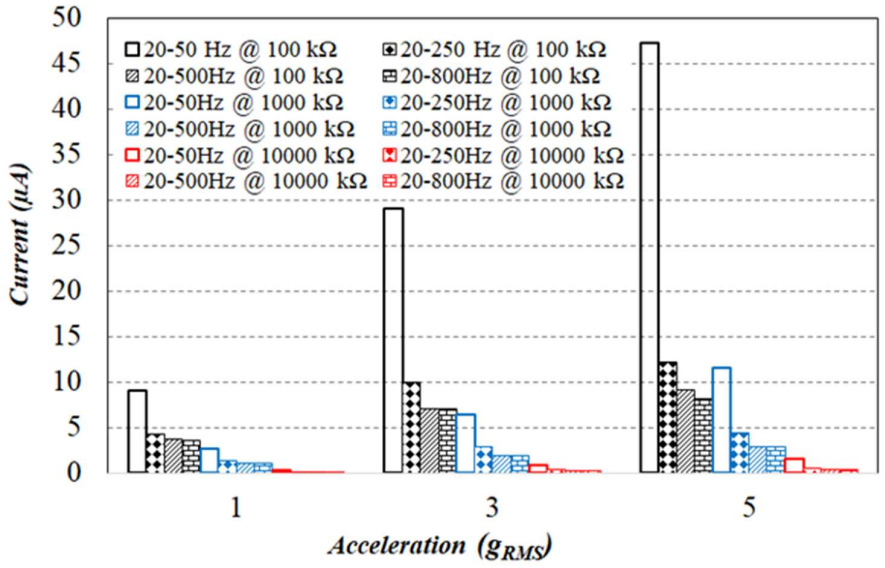

(b) Output Current

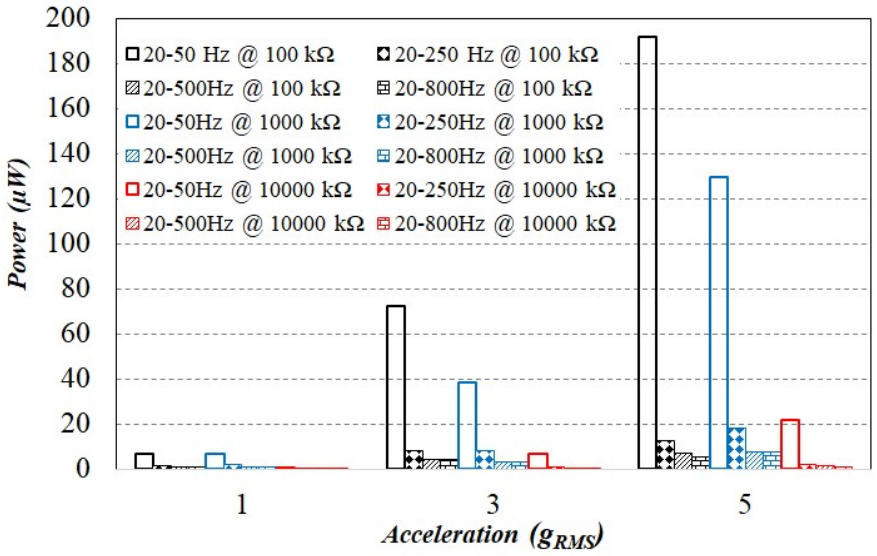

(c) Power generated

Figure 7.8. Acceleration response (random excitation) of CEH mounted in airframe

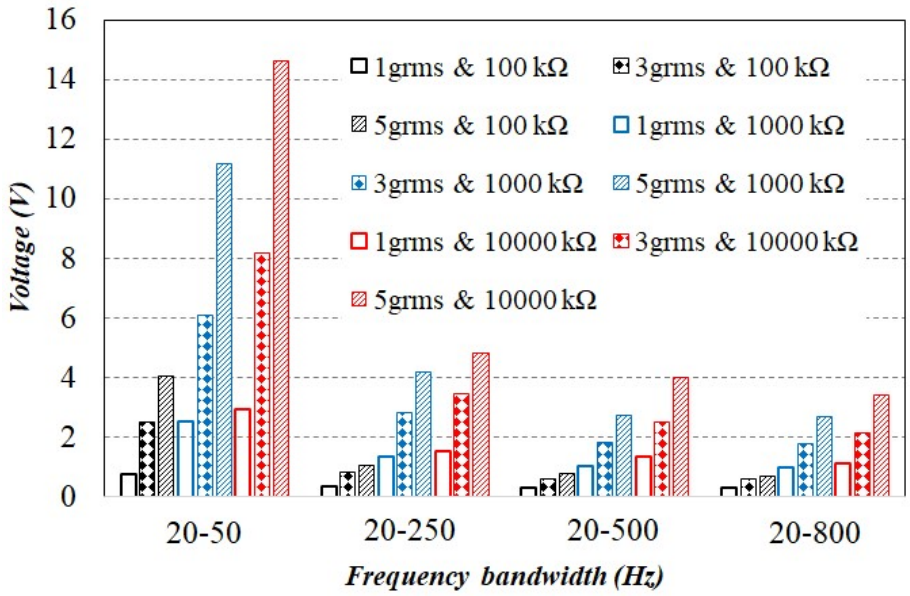

(a) Voltage across CEH

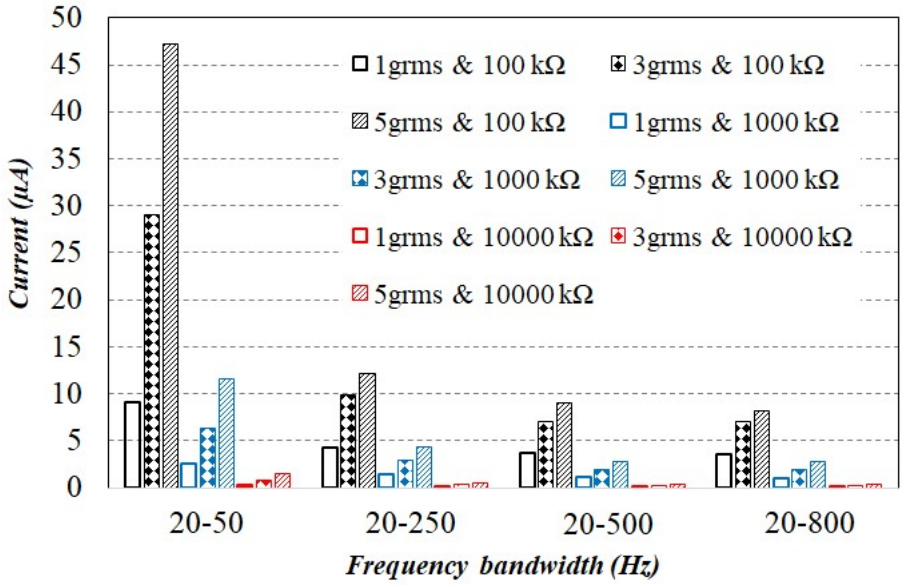

(b) Output Current

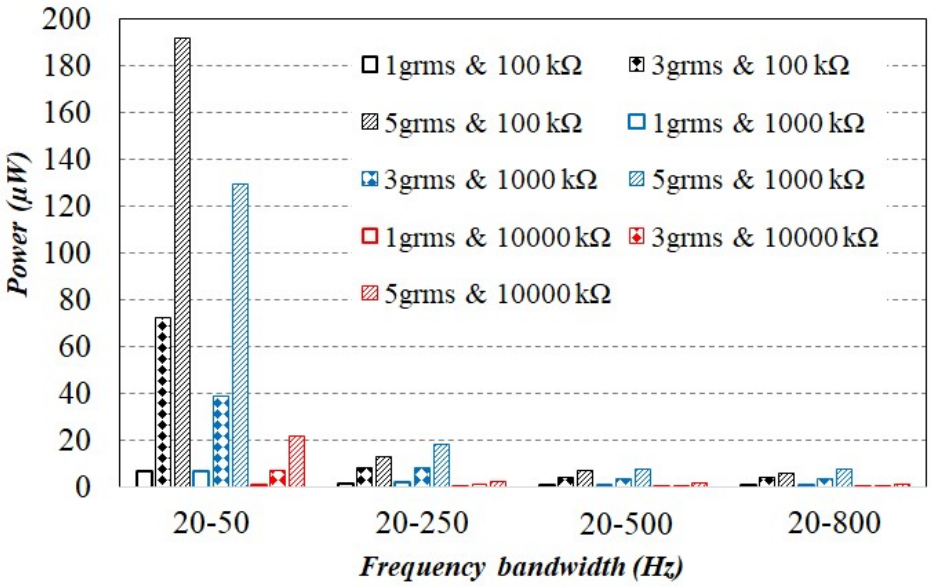

(c) Power generated

Figure 7.9. Frequency bandwidth response (random excitation) of CEH mounted in airframe

7.4. Comparison of harvested energy under harmonic and random vibrations

The power generated by CEH mounted in airframe section under the influence of harmonic and random vibrations and connected to three different loads are recorded. It is to be noted that the random excitation is given to the system at four bandwidths that is 20-50Hz, 20-250Hz, 20-500 Hz and 20-800Hz. The comparison of energy harvested during random excitation in bandwidths of 20-50Hz and 20-800 Hz which are smallest and largest in the experiment with harmonic excitation are shown in Figures 7.10(a-c) and 7.11(a-c). These comparisons clearly demonstrate that random excitation with small frequency bandwidth yields higher power output as compared to that in the case of large frequency bandwidth. It is also demonstrated that the power generated in the former case is comparatively higher than that in harmonic excitation unlike the latter case in which power generated in harmonic excitation is more than that in the case of random excitation.

The Figure 7.12 (a) and (b) shows the power ratio of random excitation in lowest frequency bandwidth – to – equivalent harmonic excitations and largest frequency bandwidth – to – equivalent harmonic excitations for three loads. The power generated during random vibration in lowest bandwidth is 2.6-12 times higher for 100 kΩ, 3.2-9 times higher for 1000 kΩ and 1.6-3 times higher for 10000 kΩ as compared to that under equivalent harmonic base excitation where as in largest bandwidth the power generated during harmonic excitations is 2.38-2.78 times higher for 100kΩ and 4.16-5.88 times higher for 10000 kΩ compared to that under random excitation. This demonstrate that maximum power can be generated when the energy harvester is installed on structures experiencing random as well as harmonic vibrations depending on the frequency bandwidths. Lower the frequency bandwidth, higher the power generated in random vibration and higher the frequency bandwidth higher the power generated in harmonic vibration. The values of voltage across the circuit, current and power generated by CEH when subjected to harmonic and random vibration is summarized in Tables 7.3 and 7.4 with increasing load resistances and base accelerations.

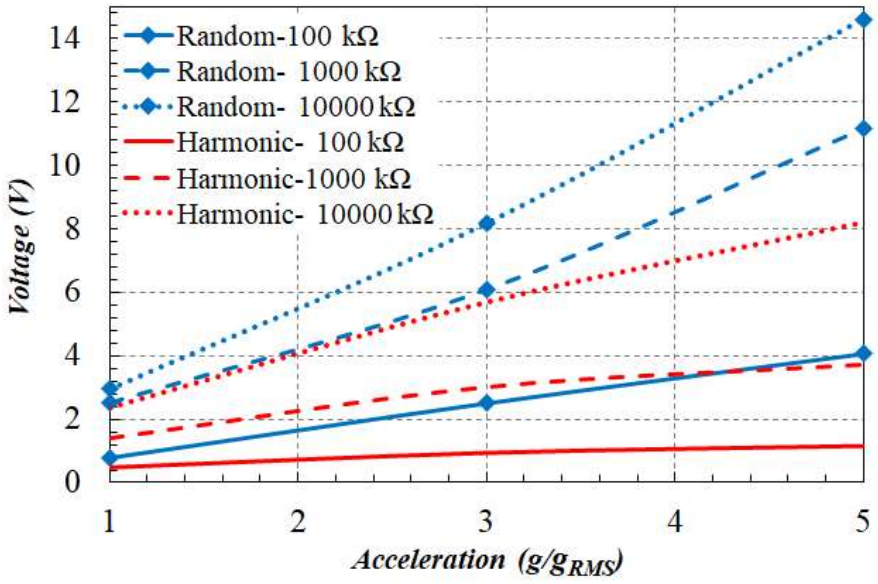

(a) Voltage across CEH

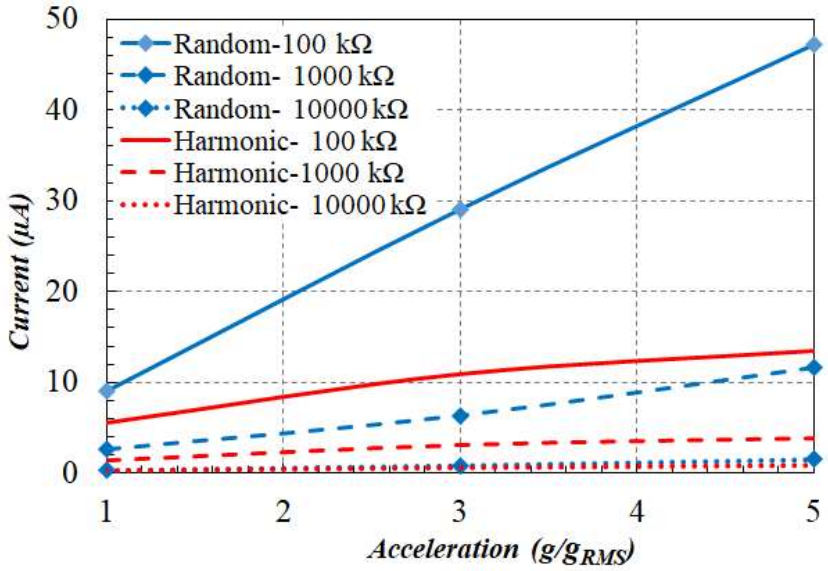

(b) Output Current

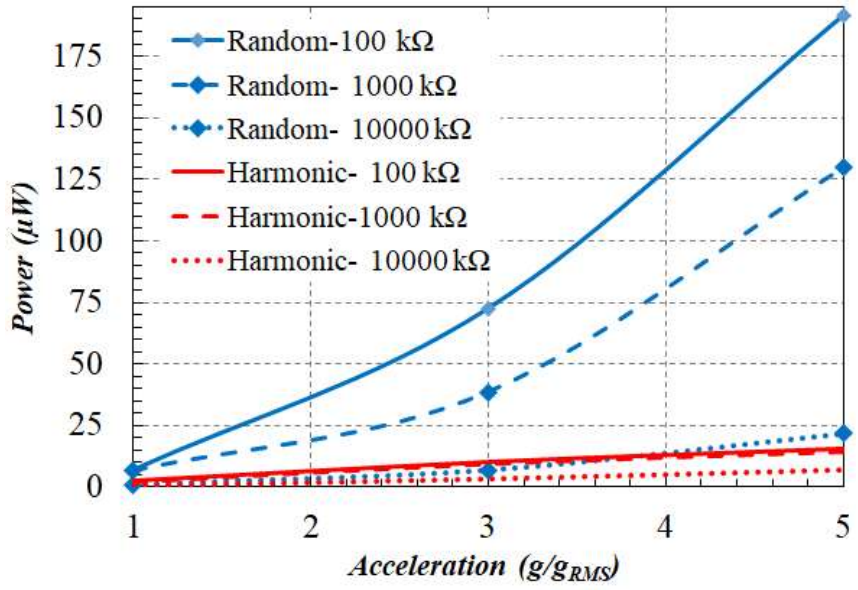

(c) Power generated

Figure 7.10. Comparison of acceleration response of CEH in airframe under harmonic and random (20-50Hz) excitations

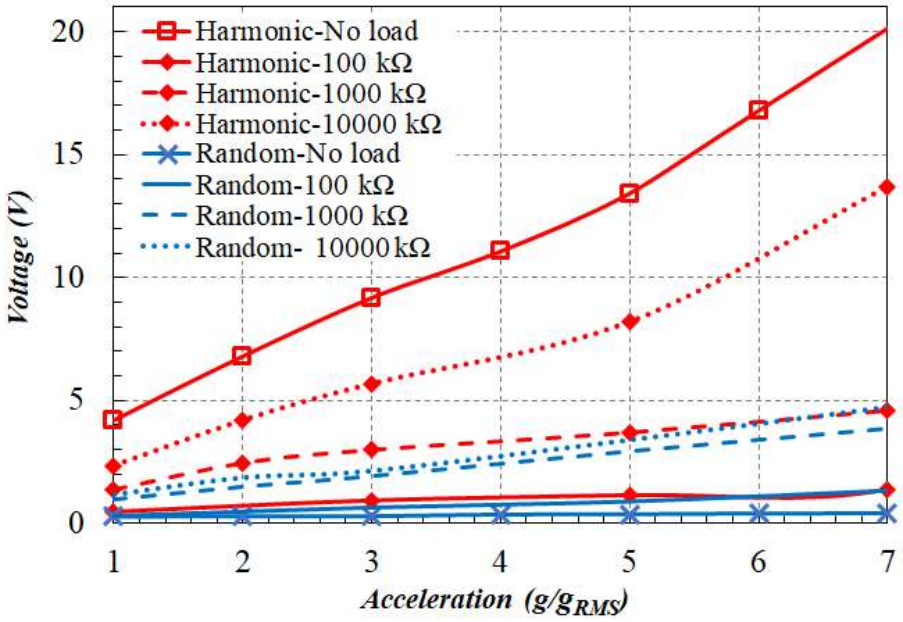

(a) Voltage across CEH

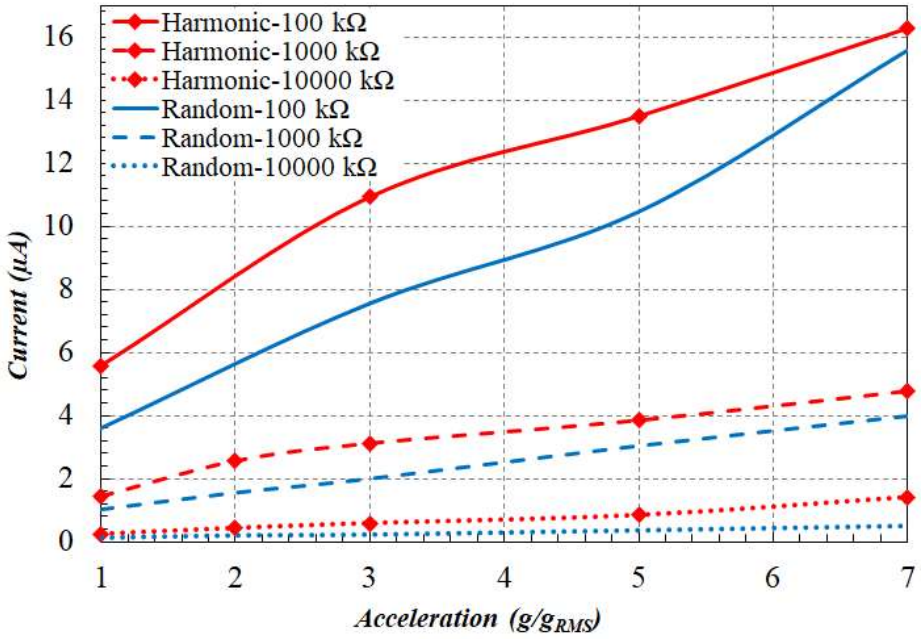

(b) Output Current

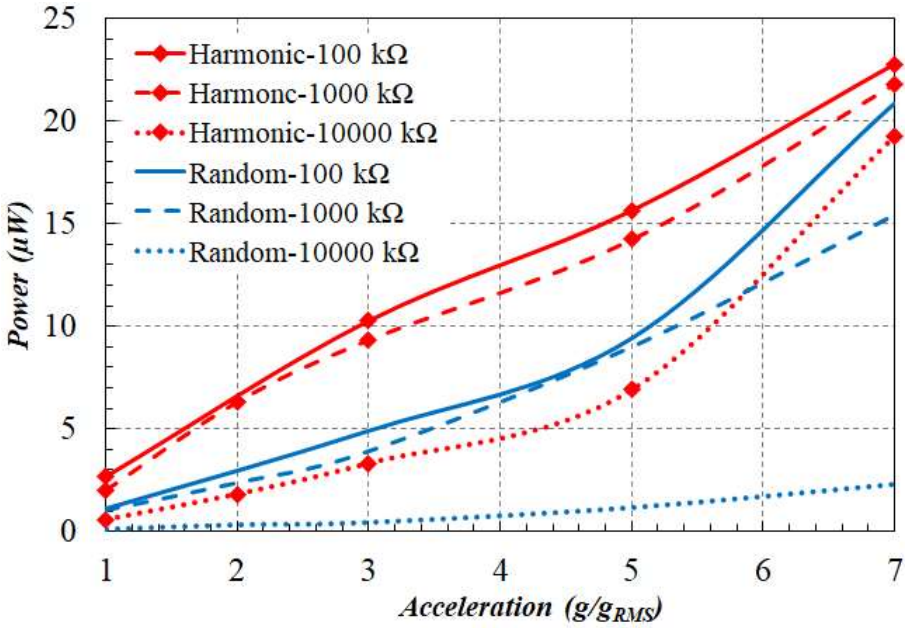

(c) Power generated

Figure 7.11. Comparison of acceleration response of CEH in airframe under harmonic and random (20-800Hz) excitations

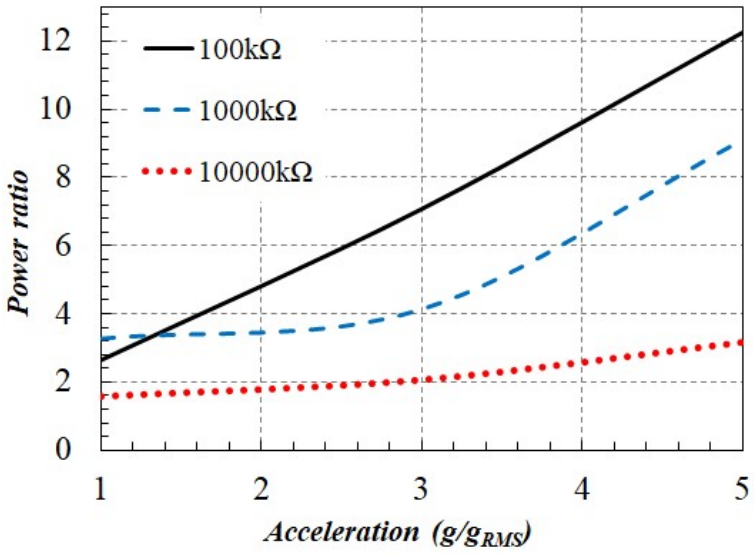

(a) Power ratio of random and equivalent harmonic excitation in 20-50Hz frequency bandwidth

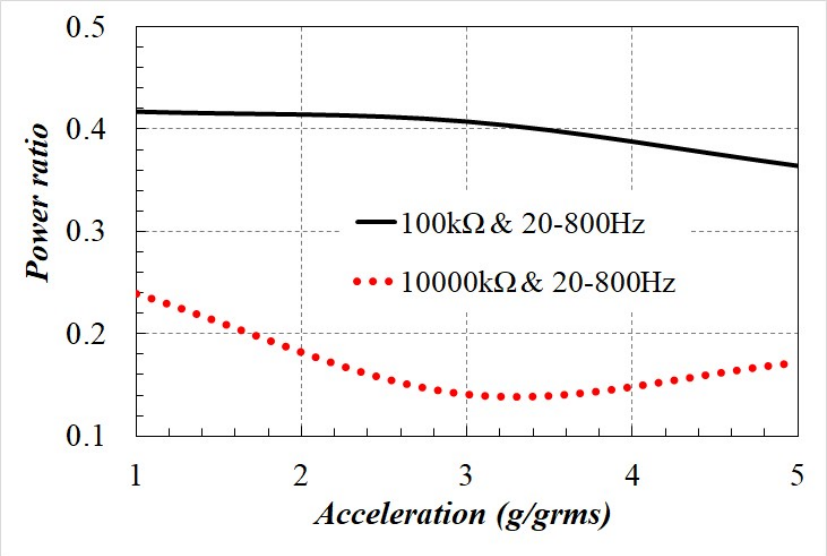

(b) Power ratio of random and equivalent harmonic excitation in 20-800Hz frequency bandwidth

Figure 7.12. Power ratio of random and equivalent harmonic excitations

Table 7. 3. Energy harvested under harmonic and random excitations: Acceleration -1g to 5g; Frequency bandwidth: 20-50 Hz

S.No.	Load (kΩ)	Harmonic excitation			Random excitation		
		Voltage (V)	Current (μA)	Power (μW)	Voltage (V)	Current (μA)	Power (μW)
1	100	0.48 – 1.16	5.6 – 13.5	2.6 – 15.6	0.78 – 4.06	9.06 – 47.2	7.0 – 191.0
2	1000	1.4 – 3.7	1.40 – 3.8	2.0 – 14.2	2.5 – 11.17	2.6 – 11.6	6.6 – 129.7
3	10000	2.35 – 8.2	0.2 – 0.8	0.56 – 6.9	2.96 – 6.60	0.3 – 1.5	0.9 – 21.9

Table 7. 4. Energy harvested under harmonic and random excitations: Acceleration-1g to 5g; Frequency bandwidth: 20-800 Hz

S.No.	Load (kΩ)	Harmonic excitation			Random excitation		
		Voltage (V)	Current (μA)	Power (μW)	Voltage (V)	Current (μA)	Power (μW)
1	100	0.48 – 1.16	5.6 – 13.5	2.6 – 15.6	0.3 – 0.7	3.6 – 8.1	1.1 – 5.7
2	1000	1.4 – 3.7	1.40 – 3.8	2.0 – 14.2	1.0 – 2.7	1.0 – 2.8	1.0 – 7.5
3	10000	2.35 – 8.2	0.2 – 0.8	0.56 – 6.9	1.15 – 3.4	0.1 – 0.35	0.13–1.18

7.5. Summary

This chapter investigated the performance of CEH mounted in airframe section subjected to harmonic and random excitations. The airframe assembly was subjected to random excitation in four different frequency bandwidths which are having same amplitude of acceleration (g_{RMS}). In this study, more clarity is obtained about the amount of power generated under the influence of random excitation as compared to that in equivalent harmonic excitations which was not understood in literature. The present research highlighted the work carried out for quantification of energy harvested under harmonic excitations at natural frequency of CEH and random excitation in different frequency bandwidths. This is done by conducting experiments on CEH by subjecting it to the increasing values of excitation (1g to 5g) for different loads 100kΩ, 1000 kΩ and 10000 kΩ. Subsequently, the experiments on CEH are extended to study the relative performance under harmonic and equivalent random excitations in different frequency bandwidths. The following important conclusions can be drawn from the present chapter.

- The results indicate that the voltage and power generated is maximum when the frequency of base excitation matches with the natural frequency of CEH (34.5 Hz) whether it is in stand-alone mode or assembled to any structure. The natural frequency of airframe and CEH are 876 Hz and 34.5 Hz respectively.

- The voltage generated by CEH is relatively high when excited in stand-alone mode than in assembled condition. The loss of voltage across CEH in assembled condition may be attributed to the damping properties of airframe structure.
- The voltage across CEH increases with increase in load resistance and the harvested current and power decrease with increase in load resistance irrespective of type of excitation.
- The voltage across CEH, output current and power generated is relatively higher when it is subjected to random excitation in a smaller bandwidth with low frequencies (20-50Hz) compared to larger bandwidth with high frequencies (20-800Hz).
- The increase in power generated by CEH connected to different loads under the influence of increasing magnitude of random vibration in smaller frequency bandwidth is relatively higher than in simple harmonic excitation which is recorded as 1.6-12 times.
- The increase in power generated by CEH connected to different loads and subjected to increasing magnitude of harmonic motion is comparatively higher than that during random excitation in larger frequency bandwidth and quantified as 2.4-5.8 times.
- It is recommended that the cantilever energy harvester can be used for aerospace applications like missiles and rockets in smaller frequency bandwidth that includes its own natural frequency.

8

Summary, Conclusion and Future Work

8.1. Introduction

Considerable understanding has been obtained from the work done in previous chapters. The feasibility of energy harvester for the application in aerospace industry is studied. This chapter summarizes the studies discussed in this thesis, conclusions drawn from the complete work and scope of work for the future.

8.2. Summary

Relying on batteries that generate power from electro-chemical reactions have significant limitations in terms of their maintenance and use in aerospace applications. Few of the limitations can be (a) charging and discharging of batteries regularly, (b) disposal of chemical waste after the shelf life of battery, (c) timely replacement of primary batteries, (d) slow rate of installation, and (e) separate cables for communication. These systems are required to be operated only when the flight vehicle is in motion. The mass of the complete vehicle can be brought down to increase the range by resizing the existing battery and removing the cables. There is also a binding need to reduce the maintenance time and cost of the systems based on battery and electrical cables for power supply and communication. This can be achieved by

using the wireless systems. The installation of these systems can be simple and fast. The configuration can be flexible. All these can be done by tapping energy available in the ambience. The sources for the ambient energies may be vibration, temperature, light and fluid flow. The focus of the present study is on tapping the energy from vibration.

The aerospace vehicle is subjected to undesired vibrations mainly due to aerodynamic disturbances and its propulsion systems. The aerodynamic disturbances are uncertain depending upon the density of air and atmospheric pressure at a particular altitude and hence random in nature. The propulsion system can induce base excitations due to (a) engine which has a compressor and nozzle that causes vibration which is harmonic in nature, and (b) solid and liquid propulsion systems which the carry fuel and oxidizer. The solid and liquid propulsion engines will generate vibrations which are random in nature along with thrust. There existed a research gap on behavior of energy harvesting structure (EHS) under the influence of random vibration and on the characterization of EHS for maximum power output under random vibration. In addition, there is no literature available on performance of EHS under the influence of both harmonic and random vibration. These gaps in research motivated not only to quantify the energy harvested from random vibrations that are caused due to aerodynamic disturbances and propulsion but also tried to consider these undesired vibrations as boon instead of penalty. In order to understand the behavior of EHS under random excitation and to evaluate the performance of EHS under random and equivalent harmonic excitations with same energy, studies are carried out by using a cantilever energy harvester.

The procedure for numerical simulation of cantilever energy harvester was established and compared with results from literature. This has been subsequently extended for the actual problem. The difference between the problem taken for reference during initial studies and actual problem is the geometry of the harvesting structure. The configuration and specification of piezoelectric material used in literature are not available in market and hence the actual problem was solved using the piezoelectric material available in market. Initially, the studies were carried out numerically on CEH subjected to harmonic motion and validated the procedure using experiments. Investigated the behavior of energy harvester when connected to different resistive loads and subjected to different magnitudes of excitations. It was explored that the available FEM tools does not have the module where the CEH can be subjected to random vibrations. Therefore, the experiment on CEH under the influence of harmonic excitation was

validated by numerical results whereas the experimental procedures were extended to study the behavior of CEH under random excitation. The behavior of CEH was studied when it was connected to different resistive loads and subjected to different magnitudes of vibration. After understanding the behavior of CEH in stand-alone mode under different conditions of harmonic and random vibrations, studies were extended on CEH mounted in an airframe section, a practical application and subjected to harmonic and random excitation. The conclusion from studies on CEH in terms of numerical simulation and experiments are mentioned in the next section.

8.3. Conclusions

The harvested energy is maximum when the harvester is in resonance with base excitation. The harvested energy increases with increase in magnitude of excitations. The voltage across the circuit, current and power generated by energy harvester increases with increase in base acceleration. Under increasing load resistance at any given base acceleration, the harvested voltage increases and the current and power decrease. The decrease in power harvested with increase in load resistance under harmonic excitation is predominantly distinguishable with increasing base acceleration. When the proof mass is increased from 0 to 1000 mg, the natural frequency monotonically follows a decreasing trend irrespective of beam width. The natural frequency with a given proof mass is lower for lower beam width and higher for higher beam width whereas the power output increases with decrease in beam width when the proof mass is increased from 200 mg to 1000 mg.

The stresses that are predominant when the harvester is exposed to acceleration are bending stresses in PZT-5A and structural steel, and shear stress in mid - adhesive plane. These stresses increase linearly with respect to proof mass and reduction in beam width. These are well within the permissible limits at 1 g base acceleration. The feasible options analyzed for maximum performance of the harvester reveals that the harvester generates a maximum power output of 880 mW and a maximum voltage of 140 V at a load of 12 kΩ when the beam width = 10 mm, proof mass = 500 mg, and resonant frequency of structure = 77.5 Hz, when exposed to the base acceleration of 30 g. It is inferred from the investigation that, with the increase in load resistance, the voltage across the circuit increases whereas the current and generated power decreases. The decrease in power output with increase in load resistance is predominantly visible with increase in base accelerations, and with increase in base accelerations, the voltage, current and power increases.

The harvested energy increases with increase in magnitude of base excitation irrespective of the type of excitation. Under increasing load resistance at any given base acceleration, the harvested voltage increases and the current and power decrease in the case of harmonic excitation, whereas the harvested voltage and power increase and the current decreases in the case of random excitation. The increase in power harvested is 2-14 times higher in random excitations as compared to equivalent harmonic excitations, with increase in equivalent base accelerations ranging from 1g to 8g for three different loads adopted in experiments. The cantilever energy harvester is recommended to be used in aerospace structures where random vibration amplitude is higher, to harvest more energy. The results indicate that the voltage and power generated is maximum when the frequency of base excitation matches with the natural frequency of CEH (34.5 Hz) whether it is in stand-alone mode or assembled to any structure. The natural frequency of airframe (Structure) and CEH are 876 Hz and 34.5 Hz respectively. Unlike aerospace vehicles, the cars and boats generate low frequency range and high amplitude vibrations for which the Electromagnetic and Electrostatic transducer based energy harvesters are best suited.

The voltage generated by CEH is relatively high when excited in stand-alone mode than in assembled condition. The loss of voltage across CEH in assembled condition may be attributed to the damping properties of airframe structure. The voltage across CEH increases with increase in load resistance and the harvested current and power decrease with increase in load resistance irrespective of type of excitation. The voltage across CEH, output current and power generated is relatively higher when it is subjected to random excitation in a smaller bandwidth with low frequencies (20-50Hz) compared to larger bandwidth with high frequencies (20-800Hz). The increase in power generated by CEH connected to different loads under the influence of increasing magnitude of random vibration in smaller frequency bandwidth is relatively higher than under harmonic excitations which is recorded as 1.6-12 times. The increase in power generated by CEH connected to different loads and subjected to increasing magnitude of harmonic excitation is comparatively higher than that during random excitation in larger frequency bandwidth and quantified as 2.4-5.8 times.

The following important conclusions can be summarized from this thesis.

- The harvested energy is maximum when the harvester is in resonance with the base excitation. The harvested energy increases with increase in base accelerations.

- Under increasing load resistance at any given base acceleration, the harvested voltage increases and the current and power decrease in the case of harmonic excitation, whereas the harvested voltage and power increase and the current decreases in the case of random excitation.
- The voltage generated by CEH is relatively high when excited in stand-alone mode than in assembled condition.
- The voltage across CEH, output current and power generated is relatively higher when it is subjected to random excitation in a smaller bandwidth with low frequencies (20-50Hz) compared to larger bandwidth with high frequencies (20-800Hz).
- It is recommended that the cantilever energy harvester can be used for aerospace applications like missiles and rockets in smaller frequency bandwidth that includes its own natural frequency.

8.4. Future Work

The following suggestions can be considered for the future extension of research.

- The aerospace vehicle is exposed to random vibration with frequency bandwidth lying between 20–2000 Hz. Studies on energy harvester configured with multiple cantilever beams may be carried out in such a way that each beam can be featured with or without proof/tip mass such that the natural frequency of beams fall within 20 - 2000 Hz.
- In the present study the CEH provides AC supply leading to AC current and power. According to the literature, rectification circuit may be designed and implemented in the CEH in order to have regulated DC supply that is mostly used for physical applications.
- Concept of super capacitor is not explored and may be studied for storing the energy harvested from CEH.
- Life studies of CEH may be explored.

References

1. “Energy harvesting through Piezoelectric materials”, Computation intelligence applications to renewable energy, 2012.
2. L. Tang, Y. Yang, C. K. Soh, “Toward Broadband Vibration-based Energy Harvesting”, *Journal of Intelligent Material System and Structures,* pp. 1867-1897, 2010.
3. H. Fang, J. Liu, Z. Xu, L. Dong, L. Wang, D. Chen, B. Cai, Y. Liu, "Fabrication and performance of MEMS-based piezoelectric power generator for vibration energy harvesting", *Microelectronics Journal 37,* p. 1280–1284, 2006.
4. J. Feenstra, J. Granstrom, H. Sodano, "Energy harvesting through a backpack employing a mechanically amplified piezoelectric stack", *Mechanical Systems and Signal Processing 22,* p. 721–734, 2008.
5. D.A. Wang, H.H. Ko, "Piezoelectric Energy Harvesting from Flow Induced Vibrations", *Journal of micromechanics and microengineering 20,* p. 025019, 2010.
6. M. Ferrari, V. Ferrari, M. Guizzetti, D. Marioli, "A Single-Magnet Nonlinear Piezoelectric Converter for Enhanced Energy Harvesting from Random Vibrations", in *Eurosensors XXIV*, 2010.
7. H. Liu, C. Quan, C. Tay, T. Kobayashi, C. Lee, "A MEMS based piezoelectric cantilever patterned with PZT thin film array for harvesting energy from low frequency vibrations", *Physics procedia 19,* pp. 129-133, 2011.
8. A. Messineo, A. Alaimo, M. Denaro, D. Ticali, "Piezoelectric Bender Transducers for Energy Harvesting Applications", *Energy Procedia 14,* p. 39 – 44, 2012.
9. N.H. Diyana, Asan G.A. Muthalif, M.N. Fakhzan, A.N.Nordin, "Vibration Energy harvesting using single and comb-shaped piezoelectric beam structures: Modeling and Simulation", in *International Symposium on Robotics and Intelligent Sensors*, 2012.
10. X. Chen, T. Yang, W. Wang, X. Yao, "Vibration energy harvesting with a clamped piezoelectric circular diaphragm", *Ceramics International 38S,* p. S271–S274, 2012.
11. L. Zhou, J. Sun, X.J. Zheng, S.F. Deng, J.H. Zhao, S.T. Peng, Y. Zhanga, X.Y. Wang, H.B. Cheng, "A model for the energy harvesting performance of shear mode piezoelectric cantilever", *Sensors and Actuators A 179,* p. 185– 192, 2012.
12. MA. Ahmad, H.N. Alshareef, "Energy harvesting from radio frequency propagation using piezoelectric cantilevers", *Solid-State Electronics 68,* p. 13–17, 2012.

13. J. Y. Noh, G. H. Yoon, "Topology optimization of piezoelectric energy harvesting devices considering static and harmonic dynamic loads", *Advances in Engineering Software 53,* p. 45–60, 2012.
14. H. Wang, Q. Meng, "Analytical modelling and experimental verification of vibration-based piezoelectric bimorph beam with a tip-mass for power harvesting", *Mechanical Systems and Signal Processing,* 2012.
15. W. Ashtari, M. Hunstig, T. Hemsel, W. Sextro, "Enhanced energy harvesting using multiple piezoelectric elements: Theory and experiments", *Sensors and Actuators A,* 2013.
16. M.N. Fakhzan, Asan G.A. Muthalif, "Harvesting vibration energy using piezoelectric material: Modeling, simulation and experimental verifications", *Mechatronics 23,* p. 61–66, 2013.
17. J. Lim, S. Jeong, N. Kim, S. Cheon, M. Kim, Tae-Gone Park, Design and fabrication of a cross-shaped piezoelectric generator for energy harvesting", *Ceramics International,* 2012.
18. X. li, K. Chuang, H. Tzou, " Energy harvesting using a circular cylindrical shell laminated with a segmented piezoelectric layer", *Proceedings of the 2010 Symposium on Piezoelectricity, Acoustic Waves and Device Applications*, 2010.
19. S. Zhao, "Energy Harvesting from Random Vibrations of Piezoelectric Cantilevers and Stack", MS thesis, Georgia Institute of Technology, 2013.
20. G. Quaranta, F. Trentadue, C. Maruccio, G. C. Marano, "Analysis of piezoelectric energy harvester under modulated and filtered white Gaussian noise", *Mech System and Signal Processing 104,* p. 134–144, 2018.
21. G. C. Marano, G. Quaranta, F. Trentadue, L. He, G Acciani, "Optimal design of energy harvesting from vibration subject to stochastic colored Gaussian process", *Journal of Physics Commununication 3,* p. 025008, 2019.
22. Y. Hu, T. Hu, Q. Jiang, "Coupled analysis for the harvesting structure and the modulating circuit in a Piezoelectric bimorph energy harvester", *Acta Mechanica Solida Sinica 20,* pp. 296-308, 2007.
23. M. Ferrari, V. Ferrari, M. Guizzetti, B. Andò, S. Baglio, C. Trigona, "Improved Energy Harvesting from Wideband Vibrations by Nonlinear Piezoelectric Converters", *Procedia Chemistry 1,* pp. 1203-1206, 2009.
24. X. Dai, Y. Wen, P. Li, J. Yang, M. Li, "Energy harvesting from mechanical vibrations using multiple magnetostrictive/piezoelectric composite transducers", *Sensors and Actuators A 166,* p. 94–101, 2011.

25. X. Wang, "Piezoelectric nanogenerators — Harvesting ambient mechanical energy at the nanometer scale", *Nano Energy 1,* pp. 13-24, 2012.
26. H. Shen, J. Qiu, M. Balsi, , "Vibration damping as a result of piezoelectric energy harvesting", *Sensors and Actuators A 169,* p. 178– 186, 2011.
27. H. Liu, C. Lee, T. Kobayashi, C. J. Tay, C. Quan, "Piezoelectric MEMS-based wideband energy harvesting systems using a frequency-up-conversion cantilever stopper", *Sensors and Actuators A 186,* p. 242– 248, 2012.
28. Z. Chen, Y. Yang, Z. Lu, Y. Luo, "Broadband characteristics of vibration energy harvesting using one-dimensional phononic piezoelectric cantilever beams", *Physica B 410,* p. 5–12, 2013.
29. L. Zuo, X. Tang, "Large-scale vibration energy harvesting", *Journal of Intelligent Material Systems and Structures 24,* p. 1405–1430, 2013.
30. A. Erturk, D. J. Inman. "Piezoelectric energy harvesting", John Wiley & Sons Ltd., 2011.
31. S. Timoshenko, D. Young and W. Weaver, "Vibration problems in Engineering", New York: John Wiley & Sons, 1974.
32. "COMSOL Multiphysics", User's Manual, Release 4.4," USA, 2013.
33. E. Lefeuvre, D. Audigier, C. Richard, D. Guyoma, "Buck boost converter for sensor less power optimization of Piezoelectric energy harvester", *IEEE transaction of Power electronics,* vol. 22, 2007.
34. M. W. Hooker, "Properties of PZT- based piezoelectric ceramics between -150 to 250 deg Celsius", Virginia: Langley research centre, 1998.
35. "ANSYS Workbench User's Manual", Version 18.1, USA: ANSYS Corporation Inc., 2019.
36. E. Halvorsen, "Energy harvesters driven by broadband random vibrations", *Journal of Micro electromechanical Systems,* vol. 17 , pp. 1061-1071, 2008.
37. A. Erturk, D. J. Inman, "An experimentally validated bimorph cantilever model for piezoelectric energy harvesting from base excitations," *Smart Material & Structures,* vol. 18, p. 25009, 2009.
38. M. I. Friswell, S. Adhikari, "Sensor shape design for piezoelectric cantilever beams to harvest vibration energy", *Journal of Applied physics,* vol. 108, p. 014901, 2010.
39. A. Nechibvute, A. Chaw, P. Luhanga, "Design & characterisation of a piezoelectric bimorph energy harvesting device", *International Journal of Engineering & Technology,* vol. 3, pp. 608-614, 2013.

40. H. Yu, J. Zhou, L. Deng, Z. Wen, "A vibration-based MEMS piezoelectric energy harvester & power conditioning circuit", *Sensors,* vol. 14, pp. 3323-3341, 2014.
41. M. Zhu and S. Edkins, Analytical modelling results of piezoelectric energy harvesting devices for self-power sensors/sensor networks in structural health monitoring, *Proc. Eurosensors XXV*, September 4-7, 195 – 198, 2011.
42. G. Litak, M. I. Friswel, S. Adhikari, "Magneto-piezo-elastic energy harvesting driven by random excitations", Applied Physics Letters 96 (2010), 214103.
43. Y. Leng, D. Tan, J. Liu, Y. Zhang, S. Fan, "Magnetic force analysis & performance of a tri-stable piezoelectric energy harvester under random excitation", *J. of Sound & Vibration* 406 (2017), 146-160.
44. A. Erturk, D. J. Inman, "Issues in mathematical modeling of piezoelectric energy harvesters", *Smart Mat. & Struct.* 17 (2008), 065016.
45. Y. Shu, I.C. Lien, "Analysis of power output for piezoelectric energy harvesting Systems", *Smart Mat. & Struct.* 15 (2006), 1499 V.
46. S. Adhikari, M. I. Friswell, D. J. Inman, "Piezoelectric energy harvesting from broadband random vibrations", *Smart Mat. & Struct.* 18 (2009), 5005.
47. D. W. Wang, M. X. Liu, W. J. Qian, X. Wu, Q. Ma, Z. Q. Wu, "Parametrical Investigation of Piezoelectric Energy Harvesting via Friction-Induced Vibration", *Shock and Vibration* (2020), 6190215.
48. Y. Li, D. Yin, X. Cheng, J. Chen, A. Zhou, X. Ji, Y. Li, "Vibration energy harvesting with piezoelectric ceramics working in d_{33} mode by using a spring-mass-spring oscillator", *Journal of Applied Physics* 127 (2020), 064104.
49. Chirag Goel, G. Srinivas,"Mechanisms and applications of vibration energy harvesting in solid rocket motors", *Microsystem Technologies* 27 (2021), 3927–3933.
50. E. Taheri, M. Zhao, H. Wu, A. Munir, "Energy harvesting from inline vibration of an elastically mounted circular cylinder in oscillatory flow", *Ocean Engineering* 239 (2021), 109694.